

**Real-time analysis of soil
gas for carbon dioxide and
oxygen to identify bedrock
mineralization and
geological faults beneath
glacial deposits in central
British Columbia**

Geoscience BC Report #
2020-07

Prepared For
Geoscience BC
May 4, 2020

R.E. Lett, Geochemist, Victoria, BC
D.A. Sacco, Palmer, Vancouver, BC
B. Elder, Palmer, Vancouver, BC
W. Jackaman, Noble Exploration Services Ltd., Jordan River, BC

Executive Summary

Carbon dioxide and oxygen concentrations measured in soil gas using onsite sampling and analytical systems have successfully detected geological structures and concealed sulphide mineralization in glaciated and non-glaciated areas. These soil-gas measurements historically required either cumbersome and relatively expensive instruments or gas capture, onsite storage and later laboratory analysis. The system described herein comprises small carbon dioxide and oxygen sensors installed in a waterproof case, a battery powered pump and a hollow, steel probe. Carbon dioxide and oxygen concentrations, barometric pressure, temperature and relative humidity in atmospheric air and in soil gas are reliably measured by the sensors and the information transferred through USB cables to a laptop computer equipped with custom software. The variables are displayed graphically in real-time and recorded for further data analysis and interpretation. System set-up at a sample site, sampling of atmospheric air for calibration, sampling soil gas and data recording can generally be completed in 15 to 20 minutes.

Initial tests with the system to determine reliability and to resolve operational issues found anomalously high carbon dioxide and low oxygen levels over the Leech River fault zone: a major tectonic structure north of Jordan River, British Columbia. A second, local test determined that the diurnal variation of carbon dioxide and oxygen concentrations would not affect the reliability of survey results if sampling and soil-gas analysis was carried out between 9.00 and 17.00 hours.

Field tests over the Mouse Mountain and Shiko Lake porphyry Cu-Au occurrences in central British Columbia demonstrate that the soil-gas composition over inferred faults has higher carbon dioxide content and is more depleted in oxygen than over surrounding rocks. Analysis of B-horizon soil samples for pH and trace elements by a water leach and modified aqua-regia dissolution followed by inductively coupled plasma mass/emission spectrometry show a spatial association between the soil-gas anomalies and soil chemistry. At Mouse Mountain, soil pH and the inverse difference hydrogen factor are spatially related to soil gas $\Delta\text{CO}_2\&\text{O}_2$ anomalies suggesting an increased CO_2 flux from bedrock influences soil pH and that calcium is mobile in the soil. Lower water-soluble calcium associated with peaks in $\Delta\text{CO}_2\&\text{O}_2$ may reflect precipitation of calcium into secondary carbonate minerals in the soil and depletion from ground water. Increased levels of water-soluble sulphur from the soil are associated with the $\Delta\text{CO}_2\&\text{O}_2$ anomalies and could reflect sulphur gases such as carbonyl sulphide from oxidizing sulphides in faults. The sulphide oxidation also explains the lower O_2 concentration in the soil gas over the inferred structures at Mouse Mountain. At Mouse Mountain anomalous soil gas $\Delta\text{CO}_2\&\text{O}_2$ levels are associated with elevated soil IDH values, but there is a weak relationship with anomalous soil Cu. At Shiko Lake, however, the association between anomalous soil gas $\Delta\text{CO}_2\&\text{O}_2$ and IDH values is weaker, but the relationship to Cu, Mo, Ag and S anomalies in the soil is stronger. This difference could be explained by more structural control of the soil gas and trace metal geochemistry at Mouse Mountain and the Shiko Lake East zone, but a stronger expression of bedrock sulphides in the soil geochemistry at the Shiko Lake Quarry zone.

The soil-gas measurement system developed here is compact, field portable and reliably measures carbon dioxide and oxygen variations in soil gas. Anomalous concentrations in these gases are believed to indicate the presence of mineralized faults concealed beneath glacial sediments. Further testing of the system would determine if there are changes in carbon dioxide and oxygen over different styles of buried sulphide mineralization and varying overburden thickness. The system can also accommodate sensors for other gases, such as methane or radon, known to be associated with sulphide mineralization.

Table of Contents

Executive Summary

1.	Introduction	1
2.	Soil gas measurement system configuration.....	3
3.	Sampling and analytical methods	5
3.1	Soil gas sampling and measurements	5
3.2	Soil gas data processing	6
3.3	Soil sampling, processing and analysis.....	7
4.	System testing and field locations	10
4.1	System functionality test, Leech River Complex, Jordan River, BC	10
4.2	Diurnal variation test, Victoria BC.....	11
4.3	Field testing, central BC	11
5.	Quality control	14
5.1	Analysis of geochemical standard material	14
5.2	Analysis of field duplicates	16
6.	Results	18
6.1	System functionality	18
6.2	Diurnal variation test.....	20
6.3	Field tests	21
6.3.1	Summary statistics for soil geochemistry.....	21
6.3.2	Mouse Mountain.....	23
6.3.3	Shiko Lake	27
7.	Discussion	33
8.	Conclusions.....	35
9.	Recommendations	36
10.	Acknowledgments.....	37
11.	References	38

List of Figures

Figure 1.	Location of the Mouse Mountain and Shiko Lake study areas in central British Columbia and the Jordan River and Victoria test sites.	2
Figure 2.	The soil gas sampling and analysis system. a) Sensor unit (25 by 22 by 11 cm); b) sampling probe (1.5 m by 12.7 mm); c) pump and power source (25 by 12 by 16 cm); d) the soil gas sampling and analysis system at a field site.	4
Figure 3.	An example of GasLab 2.1® software display from the temporal analysis of soil gas and atmosphere for CO ₂ (blue line), O ₂ (orange line) and temperature (red line) at Mouse Mountain site 1101. On the graph, sections A and C are measured in atmosphere and section B is measured in soil gas. The vertical lines on the graph roughly indicate an interval when gas flow is switched from atmosphere to soil gas and then from soil gas to atmosphere. In this example, a total of 32 measurements were made over a period of about five minutes.	6
Figure 4.	Leech River test site sample locations and geology. Site 1 to 5 correspond to Leach R 1 to 5 in Appendix A1. (Simplified geology from Cui et al. 2017).	10
Figure 5.	Mouse Mountain study area, sample locations and geology (simplified geology and fault location from Schimann, 2014).	12
Figure 6.	Shiko Lake, Quarry and East zone study areas, sample locations and simplified geology (geology and fault locations from Lesage, 2011).	13
Figure 7.	Soil gas and atmospheric air CO ₂ concentrations at Leech River Site 1. Low zones are atmosphere measurements; high zones are soil gas measurements. Note the 'spike' anomaly that occurs at the beginning of each soil-gas measurement.	19
Figure 8.	Percent Δ CO ₂ &O ₂ values measured at the Leech River sites.	20
Figure 9.	Measured soil gas and atmosphere CO ₂ concentrations near Victoria, BC on August 10, 2019.	21
Figure 10.	Mouse Mountain analytical results: a) soil gas Δ CO ₂ &O ₂ in percent; b) inverse difference hydrogen ion factor (IDH); c) soil pH; and d) soil calcium (water leach extraction followed by inductively coupled plasma mass spectroscopy). Background: simplified bedrock geology from Schimann (2014). Symbol sizes for A, B and D are true proportional scales of the sample value.	25
Figure 11.	Mouse Mountain analytical results: a) soil sulphur; and b) soil copper by water leach extraction followed by inductively coupled plasma mass spectroscopy. Simplified bedrock geology from Schimann (2014). Symbol sizes are true proportional scales of the sample value.	26
Figure 12.	Soil-gas Δ CO ₂ &O ₂ in percent, inverse difference hydrogen ion (IDH) factor with Ca, Cu and S concentrations (water leach extraction followed by inductively coupled plasma mass spectroscopy in soil along the Mouse Mountain centre transect.	27
Figure 13.	Soil gas Δ CO ₂ &O ₂ in percent, inverse difference hydrogen ion (IDH) factor with Ca, Cu and S (water leach extraction followed by inductively coupled plasma mass spectroscopy) in soil along the Mouse Mountain west transect.	27
Figure 14.	Shiko Lake Quarry zone analytical results: a) soil gas Δ CO ₂ &O ₂ in percent; b) inverse difference hydrogen ion factor (IDH); c) soil pH; and d) soil Ca determined by water leach followed by inductively coupled plasma mass spectroscopy.	29
Figure 15.	Shiko Lake Quarry zone analytical results: a) soil S; b) soil Cu; c) soil Mo; and d) soil Ag. S, Cu, Mo determined by water leach followed by inductively coupled plasma mass spectroscopy. Ag determined by modified aqua-regia dissolution followed by inductively coupled plasma mass or emission spectroscopy.	30
Figure 16.	Shiko Lake East zone analytical results: a) soil gas Δ CO ₂ &O ₂ in percent; b) inverse difference hydrogen ion factor (IDH); c) soil pH; and d) soil Ca determined by water leach followed by inductively coupled plasma mass spectroscopy.	31

Figure 17. Shiko Lake East zone analytical results: a) soil S; b) soil Cu; c) soil Mo; and d) soil Ag. S, Cu, Mo determined by water leach followed by inductively coupled plasma mass spectroscopy. Ag determined by modified aqua-regia dissolution followed by inductively coupled plasma mass or emission spectroscopy. 32

List of Tables

Table 1.	Mean and relative standard deviation (RSD%) for CO ₂ and O ₂ measured at 10-second intervals in atmospheric air (column A and C) and soil-gas (column B) at Mouse Mountain site 1101.	7
Table 2.	Elements and their detection limits (DL) determined by water leach extraction followed by inductively coupled plasma mass spectroscopy.	9
Table 3.	Elements and their detection limits (DL) determined by modified aqua-regia digestion followed by inductively coupled plasma mass and emission spectroscopy.	9
Table 4.	Reported minimum detection limits (DL), mean and relative standard deviation (RSD%) for 3 CANMET standard TILL 1 samples analysed with a water leach followed by inductively coupled plasma mass spectroscopy. RSD% was not calculated for mean values at the detection limit.....	15
Table 5.	Reported minimum detection limits (DL), mean and relative standard deviation (RSD%) for 3 CANMET standard TILL 1 samples analysed with a modified aqua-regia dissolution followed by inductively coupled plasma mass and emission spectroscopy.....	16
Table 6.	The average coefficient of variation, or CV _{AVG} calculated from 4 field duplicate samples analysed by water leach followed by inductively coupled plasma mass spectroscopy. Green indicates good precision, blue indicates acceptable precision and red, marginal to poor precision. Gold, Be, Bi, Hg, Re, Sm, Ta, Te, W are excluded because all element values in the duplicate samples are at or below detection limit.....	17
Table 7.	The average coefficient of variation, or CV _{AVG} (%) calculated from 4 field duplicate samples analysed by modified aqua-regia dissolution followed by inductively coupled plasma mass and emission spectroscopy. Green indicates good precision, blue indicates acceptable precision and red, marginal to poor precision. Boron, W and S values for the duplicate samples are at or below detection limit and have not been included in the analysis.	17
Table 8.	Mean and percent relative standard deviation (RSD%) of CO ₂ , number of measurements (N), pressure, temperature and humidity measured at 10-second intervals in atmospheric air and soil gas at Leech River Site 1. Two CO ₂ measurement sequences were collected at this calibration site to test measurement reliability. Atmospheric air measurements occur before and after each soil gas determination to establish a CO ₂ background concentration.	18
Table 9.	Mean and percent relative standard deviation (RSD%) of O ₂ , pressure, temperature and humidity measured at 10-second intervals in atmospheric air and soil gas at Leech River Site 1.	18
Table 10.	Mean and of relative standard deviation (RSD%) for CO ₂ and O ₂ measured at 10-second intervals in atmosphere and soil gas for an average 2 minutes at Victoria, BC on August 10, 2019.	21
Table 11.	Summary statistics for elements determined in the Mouse Mountain and Shiko Lake soil samples by water leach followed by inductively coupled plasma mass spectroscopy (WL).....	22

Table 12.	Summary statistics for elements determined in the Mouse Mountain and Shiko Lake soil samples by a modified aqua-regia dissolution followed by inductively coupled plasma mass and emission spectroscopy (AR).	23
Table 13.	Pearson correlation matrix for select element and soil-gas concentrations, pH and inverse difference hydrogen factors (IDH) of 30 soil samples from Mouse Mountain study area (blue text: elements analysed by water leach followed by inductively coupled plasma mass spectroscopy; black text: elements analyzed by modified aqua-regia dissolution followed by inductively coupled plasma mass and emission spectroscopy). Correlation coefficients > 0.7 are identified in red text) and > 0.5 in green.....	24
Table 14.	Pearson correlation matrix for select element and soil gas concentrations, pH and inverse difference hydrogen factors (IDH) of 14 soil samples from Shiko Lake study area (blue text: elements analysed by water leach followed by inductively coupled plasma mass spectroscopy; black text: elements analyzed by modified aqua-regia dissolution followed by inductively coupled plasma mass and emission spectroscopy).Correlation scores > 0.7 are identified in red text and > 0.5 in green.....	28

List of Appendices

Appendix A Raw CO₂ and O₂ atmosphere and soil gas measurements

- GBC_Report2020-07_Appendix A1 - Leech River Soil Gas Data.xlsx
- GBC_Report2020-07_Appendix A2 - Mouse Mountain Soil Gas Data - Sites MM 1001 to 1117.xlsx
- GBC_Report2020-07_Appendix A3 - Mouse Mountain Soil Gas Data - Sites MM 1201 to 1310.xlsx
- GBC_Report2020-07_Appendix A4 - Shiko Lake Soil Gas Data - Sites SL 2101 to 2207.xlsx
- GBC_Report2020-07_Appendix A5 - Diurnal Soil Gas Test Victoria.xlsx

Appendix B Processed soil gas data

- GBC_Report2020-07_Appendix B - Soil Gas Measurement Summary.xlsx

Appendix C Mouse Mountain and Shiko Lake soil sample descriptions

- GBC_Report2020-07_Appendix C - Soil sample descriptions and soil pH measurements.xlsx

Appendix D Mouse Mountain and Shiko Lake soil geochemistry

- GBC_Report2020-07_Appendix D - Soil Geochemical Data.xlsx

1. Introduction

Geophysical surveys can identify geological faults and potentially related sulphide mineralization, but reliably identifying these features from survey data can be difficult where their signatures are masked by host rocks with similar properties, or access is hindered by overlying glacial sediments. Faults provide a pathway for the transportation of fluids, volatile compounds, nano-particles and gases upward from deeper, crustal rocks to the surface, and thus, fluctuations in soil-gas concentrations can be a result of concealed structures and oxidizing sulphide mineralization at depth. Research into using soil gases such as radon, helium, mercury, methane and carbon dioxide (CO₂) for mineral exploration started in Russia and has been carried out for over 50 years. Ovchinnikov et. al. (1972) report anomalous levels of CO₂ above mercury mineralized faults in the North Caucasus, Russia. Among possible sources for CO₂ in soil gas are deep crustal reactions (skarn formation), the aerobic oxidation of soil organic matter and the reaction of sulphuric acid from mineral sulphides (e.g. pyrite) oxidation with carbonate minerals. Typical reactions generating carbon dioxide from these sources are:

- Skarn formation – $3\text{CaMg}(\text{CO}_3)_2 + 4\text{SiO}_2 + \text{H}_2\text{O} = \text{Mg}_3[(\text{OH})_2\text{Si}_4\text{O}_{10}] + \text{CaCO}_3 + 3\text{CO}_2$
- Organic matter oxidation – $\text{CH}_2\text{O} + \text{O}_2 = \text{CO}_2 + \text{H}_2\text{O}$
- Pyrite oxidation – $4\text{FeS}_2 + 15\text{O}_2 + 8\text{H}_2\text{O} = 2\text{Fe}_2\text{O}_3 + 8\text{H}_2\text{SO}_4$
- Calcite solution – $\text{CaCO}_3 + \text{H}_2\text{SO}_4 = \text{CaSO}_4 + \text{CO}_2 + \text{H}_2\text{O}$

During oxidation reactions, carbon dioxide is generated while oxygen (O₂) is consumed, hence an increase in CO₂ and decrease in O₂ concentrations in soil gas. Carbon dioxide migration into the soil from depth may also be accompanied by changes in mineral chemistry, such as formation of secondary carbonate minerals. Hamilton *et al.* (2004) proposed an electrochemical model to explain the anomalous pH and redox potential patterns detected in the soil over oxidizing sulphides where the bedrock is concealed beneath lacustrine clay and other glacial sediments. A key feature of the electro-chemical model is development of a reduced column, or ‘chimney’, in groundwater-saturated glacial sediment above mineralization. The model predicts that soil gas CO₂ and soil pH peaks will flank the ‘chimney’ with corresponding accumulations of secondary calcium carbonate in the soil. Klusman (2009) later refined the electro-chemical model using computer modelling to predict the flux of gases, including CO₂, by diffusion in unsaturated overburden over mineralization. Smee (1998) developed a simple yet effective method for estimating the amount of the secondary calcium carbonate by calculating an inverse difference hydrogen ion index (IDH) from the difference between a soil pH measurement and a repeat measurement after the addition of hydrochloric acid. Hence, anomalous soil pH and trace element values may directly or indirectly reflect increased migration of CO₂ through the soil to the surface.

Several examples of soil-gas anomalies have been reported from the northern hemisphere, demonstrating that they are associated with a range of mineral deposit styles. Lovell et al. (1979, 1980, 1983) reported a decrease in oxygen (O₂) and an increase in CO₂ in the soil gas sampled over Pb-Zn sulphide-mineralized faults beneath thick glacial deposits in Ireland and in semi-arid to arid parts of South West United States, South West Africa and Saudi Arabia. McCarthy et al. (1986) found elevated CO₂ and CH₄ but decreased O₂ in soil gas in samples collected in overburden at a depth of 0.5 m over the Crandon massive pyrite-sphalerite-galena deposit in Wisconsin, United States. The massive sulphide mineralization was buried beneath up to 65 m of glacial deposits. Duddridge et al. (1991) observed a similar pattern of increased CO₂ and decreased in O₂ over faults in the soil gas sampled at three

glaciated sites in the United Kingdom. Highsmith (2004) proposed a model for the formation of soil-gas anomalies and described the use of a field-portable system for measuring CO₂ and O₂ in Arizona, United States. Previous studies in glaciated areas have focused on soil-gas dispersion from massive sulphide deposits and not from other styles of sulphide mineralization, such as disseminated porphyry Cu-Au deposits.

In Hale's (2010) review of the progress and status of research into the application of soil-gas chemistry to mineral exploration, it was noted that past surveys have either measured soil gas CO₂ and O₂ concentrations on-site (e.g., Lovell et al., 1980), collected a soil-gas sample for later analysis (e.g., McCarthy et al., 1986) or used a form of passive collector such as a radon detector (Gingrich, 1984). On-site analysis has the advantage of a real-time measurement, but the commercial instrumentation used for CO₂ and O₂ analysis were historically expensive and difficult to use in remote areas. The availability of small, relatively inexpensive CO₂ and O₂ sensors, such as those distributed by CO2Meter Inc.™ (<https://www.co2meter.com/>) and Vernier Software and Technology™ (<https://www.vernier.com/>), now provides an opportunity for devising and testing an economical, on-site, real-time analytical system for measuring these gases.

The purpose of this study describes the development of a cost-effective soil-gas measurement system that will aid in the detection of geologic faults and mineralization buried beneath surficial cover. This report describes the development of a compact system able to measure CO₂ and O₂ concentrations in soil gas, and testing of the system in the field by sampling soil gas and soil geochemistry over an urban site in Victoria, British Columbia (BC); a major fault near Jordan River, BC; and two drift-covered, disseminated, porphyry Cu-Au sulphide mineral occurrences with associated faults in central BC (Mouse Mountain and Shiko Lake; Figure 1).

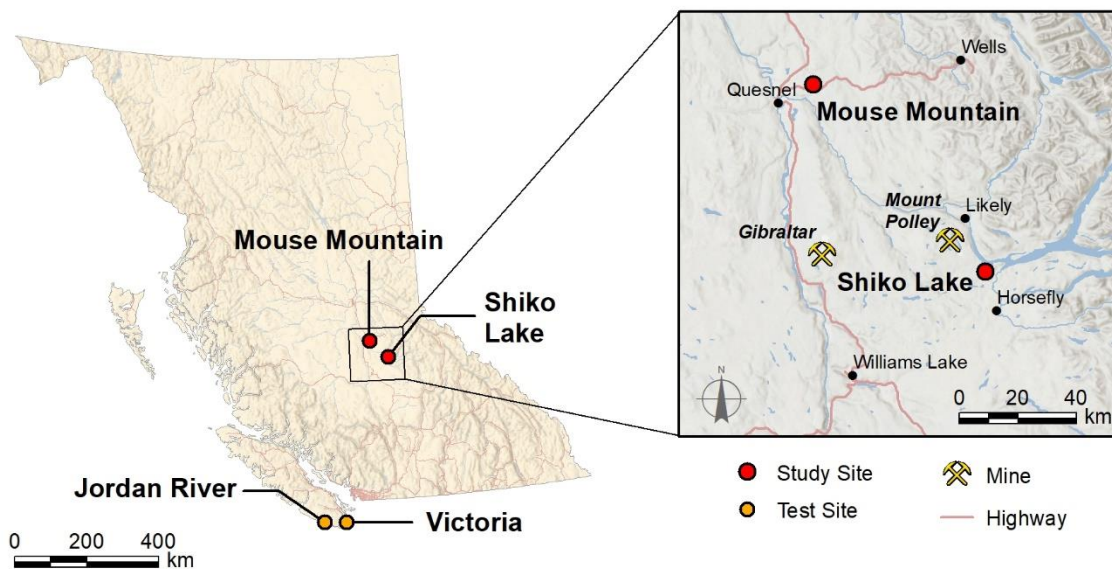


Figure 1. Location of the Mouse Mountain and Shiko Lake study areas in central British Columbia and the Jordan River and Victoria test sites.

2. Soil gas measurement system configuration

A system able to generate, reliable, real-time geochemical analyses can complement geophysical survey results and aid in bedrock mapping. Ideally, the system should be compact, portable, reliable and relatively economical to be practical for mineral exploration. Several component configurations were tested before the final system was devised; the final system components, shown in Figure 2, were purchased for roughly \$1,100.00 CAD(excluding the computer) and include:

- A CO₂ detector (SprintIR®-6S 5% CO₂ Smart Sensor) and an O₂ detector (UV Flux 25% Oxygen Smart Flow Through distributed by CO₂Meter Inc., Ormond Beach, Florida, United States). The sensors, mounted on a circuit board, measure gas concentration, barometric pressure, temperature and relative humidity. The O₂ sensor has two pressure sensors and two temperature sensors. One set of sensors is located inside the O₂ sensor module and one set is located on the board outside the sensor module. The Gaslab software reads the pressure and temperature of the gas inside the O₂ sensor. The CO₂ sensors do not have internal temperature and pressure sensors, but only have the external sensors mounted on the board. The Gaslab software reads the external pressure and temperature of the air surrounding the CO₂ sensors. The humidity sensor is mounted externally on both CO₂ and O₂ Sensors. Each sensor body has a built-in manifold with two inlet ports for attachment of flexible PVC tubes (CO₂Meter Inc. 2015). One inlet port on the CO₂ sensor manifold is connected by a PVC tube to a corresponding inlet port on the O₂ sensor so that the gas can flow continuously through the two sensors. Each sensor circuit board can be linked by USB cable to a computer. The sensors, circuit boards, PVC tube link and USB cables are installed in a waterproof case (Figure 2a).
- A sampling probe constructed from a hollow, 12.7 mm diameter, 1.5 m long steel tube fitted with a retractable, pointed tip and a hammer mounted on the tube axis to drive the tube into the overburden (Figure 2b).
- A 6-volt, battery-powered diaphragm pump designed to continuously draw soil gas through the hollow-steel-tube sampler and PVC tubing from overburden and into the sensors (Figure 2c). The soil-gas flow from the hollow-steel-tube soil sampler to the sensors is controlled by two shut-off valves (Figure 2a) that allow alternatively sampling either soil gas, for measuring CO₂ and O₂, or air, for calibrating the sensors with atmospheric CO₂ and O₂. A hydrophobic, 0.26-micron filter between the PVC tubing to the steel-tube sampler protects the sensors from particulate and soil moisture damage (Figure 2a).
- A laptop computer (not pictured) equipped with CO₂Meter.Inc GasLab 2.1 software and connected by USB cables to the CO₂ and O₂ sensor circuit boards. The GasLab 2.1 software records CO₂ and O₂ concentrations and monitors barometric pressure, temperature and relative humidity. The software displays these variables graphically and has an option for capturing digital CO₂ and O₂ concentrations for further data analysis.

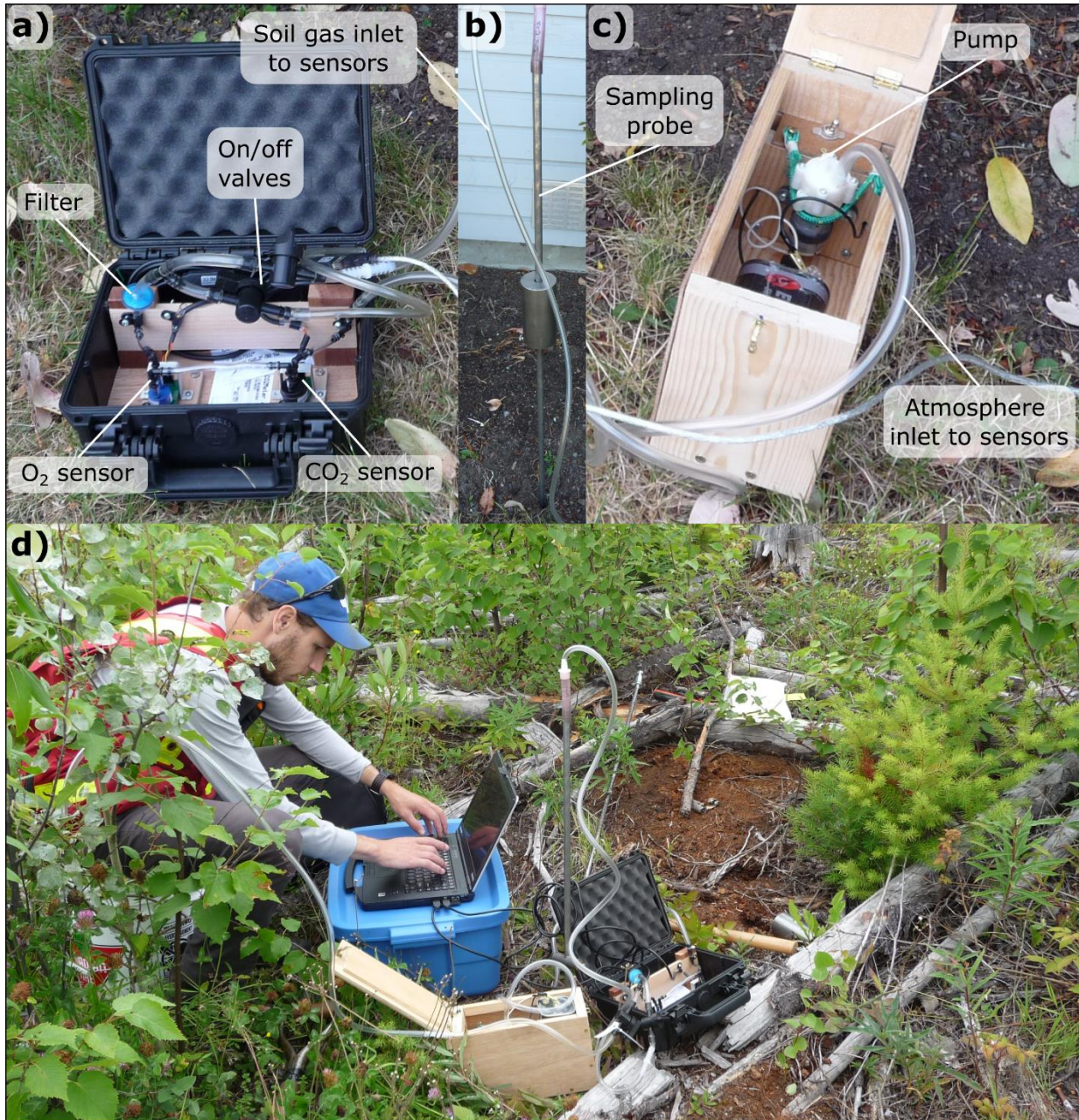


Figure 2. The soil gas sampling and analysis system. a) Sensor unit (25 by 22 by 11 cm); b) sampling probe (1.5 m by 12.7 mm); c) pump and power source (25 by 12 by 16 cm); d) the soil gas sampling and analysis system at a field site.

3. Sampling and analytical methods

3.1 Soil gas sampling and measurements

Ideally, a sample site is level, free of debris and relatively dry, as excessive soil moisture can limit gas mobility. The site location coordinates are recorded by handheld GPS, the site photographed, and the soil-gas sampling probe, pump and sensor unit assembled. Before sampling soil gas, a small hand pump is attached to the probe with PVC tubing and soil gas pumped to ensure a continuous and stable gas flow through the probe and into the measurement system. The PVC tubing with hydrophobic in-line filter and shut-off valve is attached to an inlet port on the O₂ sensor manifold. A second PVC tube, attached to an inlet port on the CO₂ sensor manifold, is connected to the diaphragm pump.

A solid, 12.7 mm diameter, pointed steel rod is first hammered into the soil to approximately 30 cm depth, avoiding boulders or bedrock. This is repeated as close as possible to the initial site if the rod encounters a large boulder or bedrock. The rod is extracted, examined for visible evidence of excess moisture and replaced by the hollow-steel-tube sampler driven farther, to 40–50 cm depth. The hollow steel tube is then carefully withdrawn 1 cm to open the retractable probe tip so that soil gas can flow into the tube. PVC tubing is connected from the sensor unit to the top of the hollow steel tube, the shut-off valve to the sensor unit is closed, the valve to the atmosphere line is opened and the electric diaphragm pump started.

After connecting the sensors to the laptop computer with the USB cables, the GasLab 2.1 software is initiated. Individual sensor settings (sensor model number, computer port) are entered and the CO₂ and O₂ measurement sequence started. Before measuring soil CO₂ and O₂ concentrations, each sensor is calibrated by the GasLab 2.1 software to atmospheric levels (CO₂ = 400 ppm, O₂ = 209,050 ppm); while there are diurnal and seasonal changes in CO₂ and O₂ concentration, CO2Meter Inc. (2015) recommends these values be used for calibration. The inlet to the atmospheric air PVC tube is positioned 3 m from the system and where possible clear of vegetation, to avoid possible human and plant influence on atmospheric measurements, and the shut-off valve to the atmosphere opened. Atmospheric CO₂ and O₂ are then measured at 10-second intervals, generally over a period of two minutes (section A in Figure 3), before the shut-off valve to the soil-gas sampler is opened and the valve to the atmosphere closed. Measurements of soil CO₂ and O₂ concentrations continue at 10-second intervals for a further two minutes. Profiles of soil-gas measurements show that CO₂ levels typically increase to a plateau and O₂ levels decrease (section B in Figure 3). Finally, the valve to the atmosphere is opened, the valve to the soil-gas sampler closed and measurements continued for two more minutes, to complete the measurement sequence (section C in Figure 3). The CO₂ and O₂ concentration, barometric pressure, temperature and relative humidity are captured by the software and recorded as a digital (.csv) text file. A full soil gas sampling and measurement sequence can generally be completed in 20 minutes.

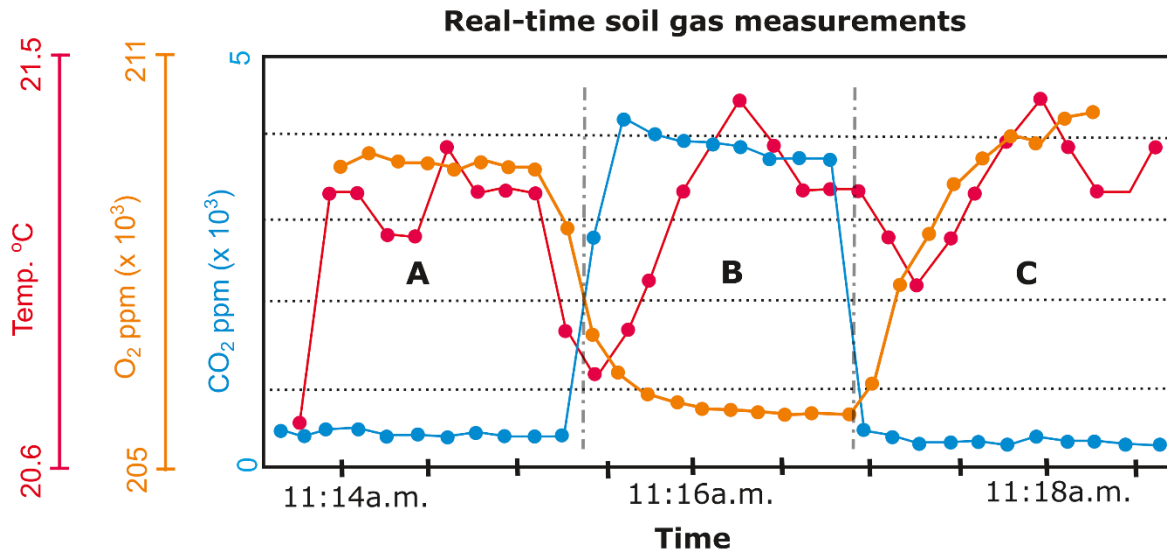


Figure 3. An example of GasLab 2.1® software display from the temporal analysis of soil gas and atmosphere for CO₂ (blue line), O₂ (orange line) and temperature (red line) at Mouse Mountain site 1101. On the graph, sections A and C are measured in atmosphere and section B is measured in soil gas. The vertical lines on the graph roughly indicate an interval when gas flow is switched from atmosphere to soil gas and then from soil gas to atmosphere. In this example, a total of 32 measurements were made over a period of about five minutes.

3.2 Soil gas data processing

Real-time graphs are produced by Gas Lab 2.1® (Figure 3) displaying CO₂ and O₂ variation. Additionally, the individual CO₂ and O₂ concentrations are measured and recorded at 10-second intervals throughout the measurement sequence. From these data the mean, standard deviation and relative standard deviation (RSD%) are calculated to estimate the precision of sensor measurements. The three sets of 10-second interval CO₂ and O₂ measurements are used to calculate the mean, standard deviation and RSD% statistics from data recorded from the two atmosphere measurements (sections A and C in Figure 3) and the soil gas measurements (section B in Figure 3). Comparison of the means in graph sections A and C shows any sensor drift during the measurement sequence, and RSD% values indicate precision of sensor measurement. Table 1 lists mean and RSD% values of CO₂ and O₂ for graph sections A, B and C from Mouse Mountain site 1101, as an example of results from a typical measurement sequence.

Table 1. Mean and relative standard deviation (RSD%) for CO₂ and O₂ measured at 10-second intervals in atmospheric air (column A and C) and soil-gas (column B) at Mouse Mountain site 1101.

Figure 3 Graph Section	A	B	C
Number of CO ₂ measurements	11	9	12
Mean of CO ₂ (ppm)	382	3766	328
RSD%	8.7	10.6	14.6
Number of O ₂ measurements	11	9	12
Mean of O ₂ (ppm)	209357	206660	209913
RSD%	0.04	0.65	0.09
Sample medium	Atmosphere	Soil gas	Atmosphere

Net soil-gas CO₂ and O₂ values representing the difference between sensor-calibrated atmospheric and measured soil-gas levels are designated ΔCO₂ and ΔO₂, and are calculated using equations 1 and 2. In the equations, the atmospheric [1] and atmospheric [2] values are mean values for the A and C datasets in Figure 3. The net ΔCO₂&O₂ concentration in soil gas (Equation 3) provides a single metric for the combined variation in CO₂ and O₂ concentrations of atmosphere and soil gases.

$$\Delta CO_2 = \text{soil gas } CO_2 - \left[\frac{\text{Atmosphere}[1] \text{ mean } CO_2 + \text{Atmosphere} [2] \text{ mean } CO_2}{2} \right] \quad (1)$$

$$\Delta O_2 = \text{soil gas } O_2 - \left[\frac{\text{Atmosphere}[1] \text{ mean } O_2 + \text{Atmosphere} [2] \text{ mean } O_2}{2} \right] \quad (2)$$

$$\text{soil gas } \Delta CO_2 \& O_2 = \Delta CO_2 + \Delta O_2 \quad (3)$$

Duplicate soil-gas CO₂ and O₂ measurements at six sites provide an estimate of combined sampling and analytical precision. At each such field duplicate site, soil gas was sampled twice from two separate holes less than 1 m apart. A coefficient of average variation, CV_{AVG} (%), calculated from six duplicate ΔCO₂ and ΔO₂ values using the equation proposed by Abzalov (2008) (Section 5.2) gives precision estimates of 18.4% for ΔCO₂, 14.0% for ΔO₂ and 15.9% for ΔCO₂&O₂. These are within the 15 to 30 CV_{AVG} % considered by Abzalov (2008) to be an acceptable level of precision. The CV_{AVG} % values for barometric pressure, temperature and humidity from the same duplicate soil-gas measurements are respectively 0.12%, 9.74% and 12.49%, which are also considered to be good precision.

3.3 Soil sampling, processing and analysis

Soil samples were collected after soil gas measurements were completed from shallow (10 to 20 cm deep), hand-dug pits adjacent to the soil gas sample site for analysis of pH and trace elements to compare soil-gas and soil geochemistry concentrations. At each site, the surface debris and humus were carefully removed, and the mineral soil sampled using a trowel from the Bm-horizon beneath the Ae-horizon (where present) and transferred into Kraft bags. Samples were approximately 500 g in size.

A 15 mL aliquot of each sample was analysed for pH to determine the inverse difference hydrogen (IDH) factor using the following method proposed by Smee (2009). At base camp (i.e., motel), small pebbles and organic debris were removed from the untreated soil, and the soil was transferred to a graduated

PVC cup. Fifteen mL of distilled water was added to the soil and agitated for 20 seconds with a plastic stir stick. The pH was measured with an Oakton pHTestr® 30 meter calibrated with pH 4, 7 and 10 buffers. One drop (0.2 mL) of 10 percent hydrochloric acid (HCl) was added and the pH was measured again after 5 seconds. The IDH factor was calculated from the two pH measurements using the inverse of the difference between the acidified and non-acidified H⁺ concentrations (Smee, 2009).

A second aliquot of each soil samples was air-dried in a contained room and sieved to minus 80 mesh size (< 0.177 mm). The dried soil and geochemical standard (CANMET till 1) samples were sent to Bureau Veritas Minerals Laboratory (Vancouver, BC) for analysis of trace and minor elements. Two analytical methods were used to discriminate, if possible, between elements associated with different mineral phases in the soil. The methods are:

- **A water leach extraction followed by inductively coupled plasma mass spectroscopy (BV LH101; referred to hereinafter as WL).** This leach extracts elements adsorbed to the surface of clay and other soil forming minerals and water-soluble minerals (Hall, 1998). For the analysis, a 1 g portion of the minus 80 mesh size-fraction was leached with distilled, deionized water for 2 hours, centrifuged and the solution analysed for 63 elements by inductively coupled plasma mass spectroscopy (ICP-MS).
- **A modified aqua-regia digestion followed by inductively coupled plasma mass and emission spectroscopy (BV AQ250; referred to hereinafter as AR).** This reagent dissolves sulphides, precious metals and many rock forming silicate minerals to release metal. For the analysis, a 0.5 g portion of the minus 80 mesh size-fraction was digested for 90 minutes in 1:1:1 solution of HNO₃-HCl-H₂O acid (modified aqua-regia) at 95°C, cooled and the solution analysed for 37 trace and minor elements by (ICP-MS/ES).

A full list of analytes and their detection limits for both methods are shown in Tables 2 and 3.

Table 2. Elements and their detection limits (DL) determined by water leach extraction followed by inductively coupled plasma mass spectroscopy.

Element	Unit	DL
Ag	PPB	0.5
Al	PPM	1
As	PPB	5
Au	PPB	1
Ba	PPB	10
Be	PPB	1
Bi	PPB	0.5
Br	PPB	10
Ca	PPM	5
Cd	PPB	0.5
Ce	PPB	1
Cl	PPM	2
Co	PPB	1
Cs	PPB	0.5
Cu	PPB	5
Dy	PPB	0.1
Er	PPB	0.1
Eu	PPB	0.1
Fe	PPM	0.1
Ga	PPB	0.5
Gd	PPB	0.1
Ge	PPB	0.1

Element	Unit	DL
Hf	PPB	0.1
Hg	PPB	1
Ho	PPB	0.05
In	PPB	0.05
K	PPM	2
La	PPB	2
Li	PPB	0.1
Lu	PPB	0.05
Mg	PPM	0.1
Mn	PPB	50
Mo	PPB	1
Na	PPM	3
Nb	PPB	0.5
Nd	PPB	1
Ni	PPB	5
P	PPM	0.1
Pb	PPB	3
Pr	PPB	0.5
Rb	PPB	2
Re	PPB	0.05
S	PPM	10
Sb	PPB	1

Element	Unit	DL
Sc	PPB	20
Se	PPB	5
Sm	PPB	0.5
Sn	PPB	1
Sr	PPB	10
Ta	PPB	0.5
Tb	PPB	0.05
Te	PPB	1
Th	PPB	2
Ti	PPM	0.05
Tl	PPB	0.2
Tm	PPB	0.05
U	PPB	0.1
V	PPB	50
W	PPB	2
Y	PPB	1
Yb	PPB	0.5
Zn	PPB	10
Zr	PPB	1

Table 3. Elements and their detection limits (DL) determined by modified aqua-regia digestion followed by inductively coupled plasma mass and emission spectroscopy.

Element	Unit	DL
Ag	PPB	2
Al	%	0.01
As	PPM	0.1
Au	PPB	0.2
B	PPM	20
Ba	PPM	0.5
Bi	PPM	0.02
Ca	%	0.01
Cd	PPM	0.01
Co	PPM	0.1
Cr	PPM	0.5
Cu	PPM	0.01
Fe	%	0.01

Element	Unit	DL
Ga	PPM	0.1
Hg	PPB	5
K	%	0.01
La	PPM	0.5
Mg	%	0.01
Mn	PPM	1
Mo	PPM	0.01
Na	%	0.001
Ni	PPM	0.1
P	%	0.001
Pb	PPM	0.01
S	%	0.02
Sb	PPM	0.02

Element	Unit	DL
Sc	PPM	0.1
Se	PPM	0.1
Sr	PPM	0.5
Te	PPM	0.02
Th	PPM	0.1
Ti	%	0.001
Tl	PPM	0.02
U	PPM	0.1
V	PPM	1
W	PPM	0.1
Zn	PPM	0.1

4. System testing and field locations

Prior to deployment on mineral exploration properties in central BC, the soil-gas system was tested near Jordan River and in Victoria, BC, to identify and resolve any basic operational issues.

4.1 System functionality test, Leech River Complex, Jordan River, BC

An initial test to determine the reliability and functionality of the system was performed by sampling soil-gas composition across the Leech River Fault Zone, 12 km north of Jordan River, BC (Figure 1). The Leech River fault zone, comprising several sub-parallel normal and thrust faults, marks the contact between basalt of Eocene Metchosin Igneous Complex to the south and the variably metamorphosed and deformed pelitic and arenaceous metasedimentary rocks of the Leech River Complex to the North (Figure 4). Soil gas CO₂ and O₂ concentrations, pressure, temperature and humidity were measured at five sites with the soil gas system along a 6 km section of logging road (Figure 4). Measurements were collected at 10-second intervals over 10 minutes. From these measurements, RSD% is calculated to estimate the precision of the results, and the data are reviewed for correlative measurements that could indicate mixing of the soil gas with atmosphere.

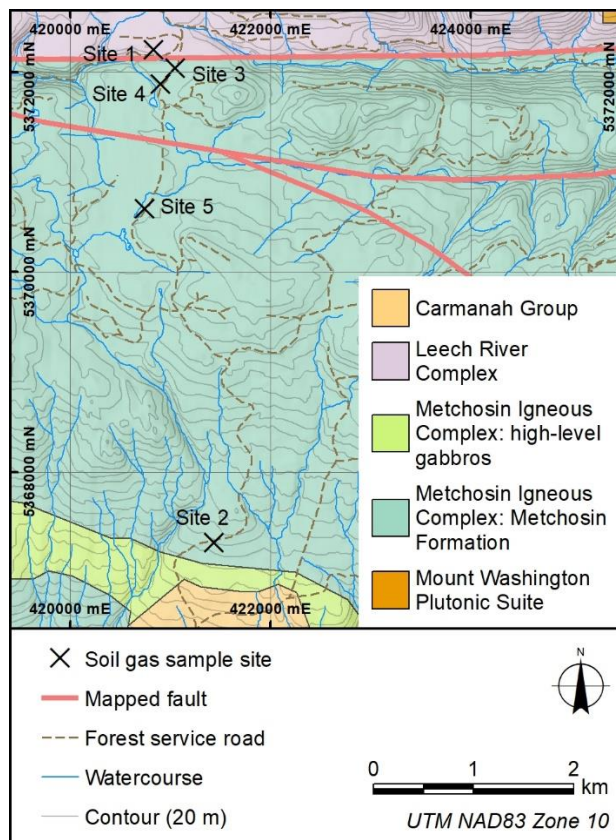


Figure 4. Leech River test site sample locations and geology. Site 1 to 5 correspond to Leach R 1 to 5 in Appendix A1. (Simplified geology from Cui et al. 2017).

4.2 Diurnal variation test, Victoria BC

Atmospheric CO₂ and O₂ levels are known to fluctuate seasonally and daily and these fluctuations could complicate the interpretation of soil-gas measurements. Seasonal fluctuations were not measured during this study. Imasu and Tanabe (2018) report a 10 ppm CO₂ annual variation during 2014 at a site on the forested Dodaira Mountain, Saitama Prefecture, Japan. This amount of CO₂ variation would not significantly change the interpretations of this study. Diurnal variation was evaluated on August 10, 2019 in Victoria, BC (Figure 1). Atmospheric and soil gas CO₂ and O₂ concentrations were measured every 2 to 3 hours between 9:00 and 22:00 hours to quantify the diurnal variation and to determine if the variation was enough to require consideration in the sampling protocols.

4.3 Field testing, central BC

Upon satisfactory system testing, two field locations were chosen in central BC based on the occurrence of faults in existing maps, Cu-Au porphyry-style disseminated sulphide mineralization and a cover of glacial drift: 1) Mouse Mountain (MINFILE 093G 003; BC Geological Survey, 2019) mineral occurrence, 13 km east of Quesnel; and 2) the Shiko Lake property (MINFILE 093A 058), 17 km north of Horsefly (Figure 1). The program was carried out in July and August of 2019. Soil-gas measurements and soil samples for pH and geochemical determinations were collected from each sample site along three transects at Mouse Mountain and two transects at Shiko Lake. The transects were designed to target inferred faults. Sampling on a regular grid (e.g., 25 m by 25 m) over the faults would have been preferable; however, uncertainty of the precise fault locations, time constraints and site access limitations necessitated a more flexible, variable sampling pattern (i.e., modified based on real-time soil-gas measurements and accessibility).

At Mouse Mountain the Valentine zone is an outcropping sulphide-mineralized zone, where Cu-Au porphyry-style disseminated chalcopyrite, pyrite and bornite are associated with Jurassic calc-alkaline plutons intruded into Upper Triassic to Lower Jurassic Nicola Group sedimentary and volcanic rocks (Figure 5). Sampling was undertaken near the Valentine zone, where Schimann (2014) describes a fractured and faulted fine-grained diorite, monzonite and syenite body in contact with potassic-altered volcanic breccia. Mineralization at the Valentine zone consists of chalcopyrite, malachite and magnetite associated with an envelope of potassic alteration (Jonnes and Logan, 2007). The presence and exact location of a northeast-southwest-trending fault identified by Schimann (2014) crossing the area south of the Valentine zone is uncertain (Figure 5). Jonnes and Logan (2007) describe a major east-striking fault zone exposed approximately 3 km west of Mouse Mountain. While the fault is shown on past geological maps to transect the monzonite, Jonnes and Logan note that there is no outcrop evidence of the structure. However, because this structure is shown on the most recent geological map of the Mouse Mountain property it is retained for interpreting the geochemistry and designated as "mapped" in figures. Bedrock is exposed at the Valentine zone but is concealed in the south under a mantle of till estimated at 2 to 3 m thickness. The south-facing slope below the Valentine zone has been disturbed by logging and has predominantly Brunisolic soils. Soil gas sampling along three transects south from the Valentine zone generated 44 soil-gas measurements from 33 sample sites; soil samples were collected at 29 sites for geochemical analysis, pH and IDH determinations (Figure 5).

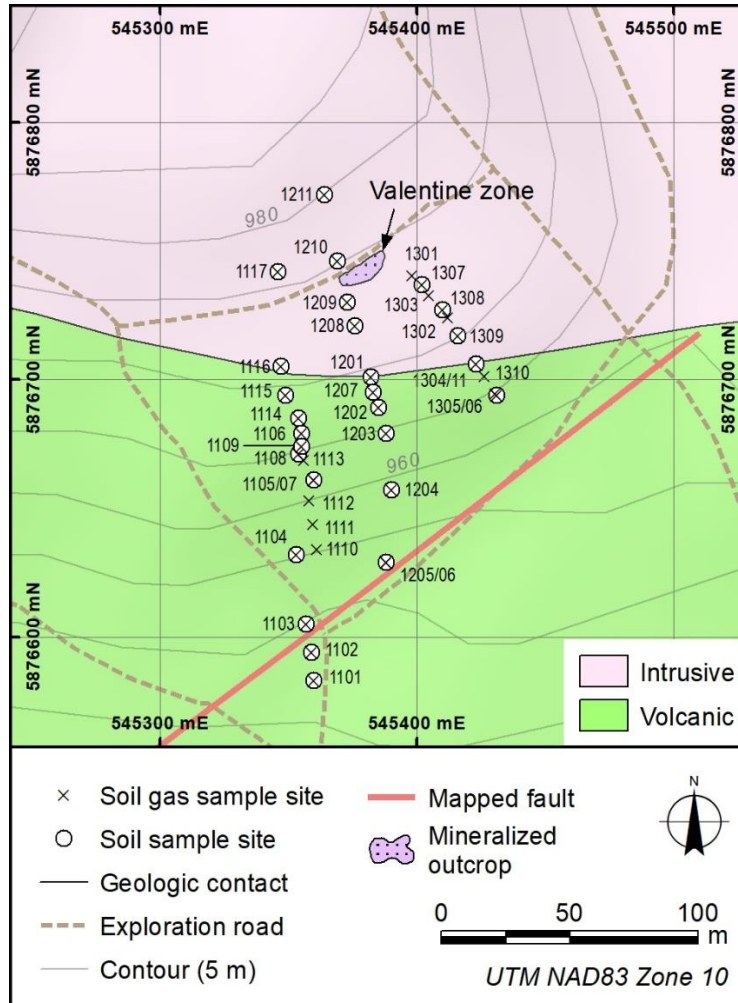


Figure 5. Mouse Mountain study area, sample locations and geology (simplified geology and fault location from Schimann, 2014).

At Shiko Lake, a diorite-syenite-monzonite stock encloses coeval and comagmatic Nicola Group augite basalt, felsic heterolithic breccia, massive to locally laminated tuff, and maroon-coloured, possibly subaerial basaltic flows (Morton, 2003; Lesage, 2011). Soil gas and soil sampling were carried out over the Quarry zone, and approximately one km to the east at the East Zone (Figure 6). Hornfelsed, pyrite-bearing siltstone in contact with diorite at the Quarry zone is covered by till estimated at 1 to 2 m thick. Mineralization at the Quarry zone consists of Au-bearing chalcopyrite and bornite in fractures and disseminated sulphides in a composite alkalic augite-monzonite-syenite intrusion. Andesite at the East zone is intersected by northeast-striking faults, interpreted from ground geophysics and geological relationships (Lesage, 2011). The bedrock is partially concealed by a 1 to 2 m thick veneer of till. Past mineral exploration and logging have disturbed the land surface. The soil formed at the Quarry and East zones is a Brunisol. Fifteen soil-gas measurements were made at the Quarry and East zones from 14 sites, and 14 soil samples were collected for geochemical analysis, pH and IDH determinations (Figure 6).

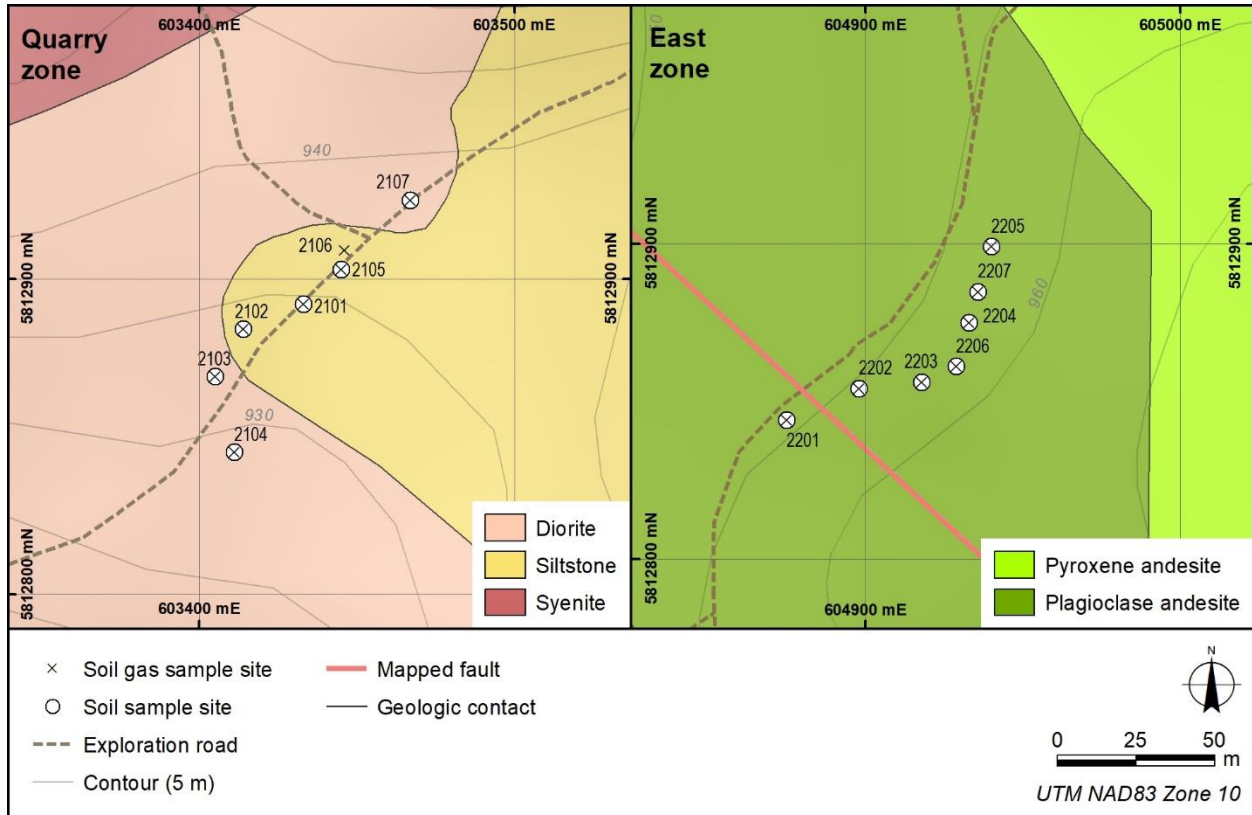


Figure 6. Shiko Lake, Quarry and East zone study areas, sample locations and simplified geology (geology and fault locations from Lesage, 2011).

5. Quality control

A reliable interpretation of geochemical data is not possible unless there is an estimate of the variability caused by the sampling and the sample analysis. The variability in terms of accuracy and precision is estimated by a statistical evaluation of the analytical results from duplicate soil samples collected at the field sites, prepared and split before analysis and with standard reference material randomly inserted into the sample sequence. The reliability of the soil gas CO₂ and O₂ measurements has been assessed in Section 3. This section evaluates the precision of the soil geochemistry analyses.

5.1 Analysis of geochemical standard material

Analytical precision is commonly expressed as the RSD% determined from the results of repeated geochemical analysis of a standard reference material. The RSD% is calculated as standard deviation of the determinations divided by the mean of the determinations multiplied by 100 to give a percentage.

Table 4 (WL) and Table 5 (AR) provide the mean and RSD% for each element. In general, an RSD% below 15 is considered acceptable (Fletcher, 1981). For the WL data, more than 50 percent of the elements show acceptable precision except for the rare earth elements, Co, Mo, Re and Cd. All WL determinations for Au, Be, Hg, Sc, Ta, Te, V and W are below detection limit, hence no RSD% are listed. The WL Cl, Hf, K and Th analyses for TILL 1 are identical and the RSD% values are shown as < 1 in Table 4. Similarly, the RSD% for the AR data indicate most elements have acceptable precision. Gold, and Te, however, have larger RSD% values suggesting greater analytical variability. The RSD% values for AR B, S, Se and W are not listed in Table 5 because all values are below detection limit. All AR U analyses for TILL 1 are identical and the RSD% is listed as < 1.

Table 4. Reported minimum detection limits (DL), mean and relative standard deviation (RSD%) for 3 CANMET standard TILL 1 samples analysed with a water leach followed by inductively coupled plasma mass spectroscopy. RSD% was not calculated for mean values at the detection limit.

Element	Unit	DL	Mean	RSD%
Ag	ppb	0.5	0.7	14.3
Al	ppm	1	14.0	12.4
As	ppb	5	28.3	10.2
Au	ppb	1	-	-
Ba	ppb	10	193.0	10.9
Be	ppb	1	-	-
Bi	ppb	0.5	3.0	10.1
Br	ppb	10	385.0	5.9
Ca	ppm	5	76.3	2.0
Cd	ppb	0.5	0.5	179.7
Ce	ppb	1	37.7	15.1
Cl	ppm	2	11.0	< 1
Co	ppb	1	10.0	20.0
Cs	ppb	0.5	0.5	-
Cu	ppb	5	219.7	4.3
Dy	ppb	0.1	2.8	13.7
Er	ppb	0.1	1.5	10.4
Eu	ppb	0.1	0.8	15.1
Fe	ppm	0.1	18.0	13.8
Ga	ppb	0.5	4.1	9.8
Gd	ppb	0.1	3.0	12.8
Ge	ppb	0.1	0.6	16.7
Hf	ppb	0.1	0.3	< 1
Hg	ppb	1	-	-
Ho	ppb	0.05	0.5	15.1
In	ppb	0.05	0.2	23.9
K	ppm	2	21.0	< 1
La	ppb	2	15.0	24.0
Li	ppb	0.1	4.1	12.4
Lu	ppb	0.05	0.2	8.6
Mg	ppm	0.1	22.9	5.8
Mn	ppb	50	4427.0	4.8
Mo	ppb	1	5.0	20.0
Na	ppm	3	45.3	2.5

Element	Unit	DL	Mean	RSD%
Nb	ppb	0.5	2.2	23.0
Nd	ppb	1	16.7	12.5
Ni	ppb	5	13.7	4.2
P	ppm	0.1	4.5	3.4
Pb	ppb	3	15.0	6.7
Pr	ppb	0.5	4.3	16.7
Rb	ppb	2	34.7	1.7
Re	ppb	0.05	0.1	30.2
S	ppm	10	19.0	15.8
Sb	ppb	1	39.3	3.9
Sc	ppb	20	-	-
Se	ppb	5	8.0	12.5
Sm	ppb	0.5	3.7	14.8
Sn	ppb	1	2.7	43.3
Sr	ppb	10	112.3	4.9
Ta	ppb	0.5	-	-
Tb	ppb	0.05	0.4	12.9
Te	ppb	1	-	-
Th	ppb	2	4.0	< 1
Ti	ppm	0.05	0.8	11.8
Tl	ppb	0.2	0.5	12.4
Tm	ppb	0.05	0.2	28.5
U	ppb	0.1	2.7	7.8
V	ppb	50	-	-
W	ppb	2	-	-
Y	ppb	1	15.3	16.4
Yb	ppb	0.5	1.6	7.4
Zn	ppb	10	50.7	12.8
Zr	ppb	1	14.0	25.8

Table 5. Reported minimum detection limits (DL), mean and relative standard deviation (RSD%) for 3 CANMET standard TILL 1 samples analysed with a modified aqua-regia dissolution followed by inductively coupled plasma mass and emission spectroscopy.

Element	Unit	DL	Mean	RSD%
Ag	ppb	2	226.0	3.8
Al	%	0.01	1.8	2.4
As	ppm	0.1	14.8	3.9
Au	ppb	0.2	8.4	46.0
B	ppm	20	-	-
Ba	ppm	0.5	76.0	8.0
Bi	ppm	0.02	1.9	4.6
Ca	%	0.01	0.3	4.9
Cd	ppm	0.01	0.2	6.3
Co	ppm	0.1	12.2	4.6
Cr	ppm	0.5	26.7	4.7
Fe	%	0.01	3.2	2.1
Ga	ppm	0.1	6.6	6.6
Hg	ppb	5	89.3	9.7
K	%	0.01	0.1	9.1
La	ppm	0.5	17.9	7.5
Mg	%	0.01	0.6	2.6

Element	Unit	DL	Mean	RSD%
Mn	ppm	1	1056.0	5.8
Na	%	0.001	0.0	6.7
Ni	ppm	0.1	18.3	6.2
P	%	0.001	0.1	3.1
S	%	0.02	-	-
Sb	ppm	0.02	4.2	2.9
Sc	ppm	0.1	4.6	3.3
Se	ppm	0.1	0.3	-
Sr	ppm	0.5	10.1	3.8
Te	ppm	0.02	0.0	21.7
Th	ppm	0.1	2.5	9.9
Ti	%	0.001	0.1	4.5
Tl	ppm	0.02	0.1	4.7
U	ppm	0.1	0.8	< 1
V	ppm	1	56.3	2.7
W	ppm	0.1	-	-

5.2 Analysis of field duplicates

Four field duplicate samples were collected and analysed by both geochemical determination methods. The average coefficient of variation (CV_{AVR}) calculated from the formula proposed by Abzalov (2008) provides an estimate of the overall sampling and analytical precision from the field duplicate data presented in Table 6 for WL data and Table 7 for AR data. In equation 4, the terms a and b represent the analyses of first and second of the duplicate sample pair and N is the number of duplicate pairs. Values can range from 0%, when duplicate pairs have identical concentrations, to an upper value above 141.42 (i.e. the square root of 2) when duplicate results exhibit maximum differences.

$$CV_{avr}(\%) = 100 \cdot \sqrt{\frac{2}{N} \sum_{i=1}^N \frac{(a_i - b_i)^2}{(a_i + b_i)^2}} \quad (4)$$

Table 6. The average coefficient of variation, or CV_{AVG} calculated from 4 field duplicate samples analysed by water leach followed by inductively coupled plasma mass spectroscopy. Green indicates good precision, blue indicates acceptable precision and red, marginal to poor precision. Gold, Be, Bi, Hg, Re, Sm, Ta, Te, W are excluded because all element values in the duplicate samples are at or below detection limit.

Element	CV_{avg} (%)						
S (ppm)	5.44	Rb (ppb)	23.24	Li (ppb)	36.95	Gd (ppb)	64.25
As (ppb)	8.01	Zr (ppb)	23.25	K (ppm)	37.87	Y (ppb)	64.77
Ti (ppm)	8.86	Ag (ppb)	23.57	Ge (ppb)	41.67	Dy (ppb)	64.83
Sr (ppb)	10.54	Ca (ppm)	23.69	Tm (ppb)	45.75	Nd (ppb)	66.23
Ni (ppb)	12.39	Al (ppm)	23.71	U (ppb)	46.48	Ho (ppb)	67.90
Cd (ppb)	12.48	Mo (ppb)	23.74	Mn (ppb)	47.86	Pr (ppb)	69.15
Mg (ppm)	14.65	Na (ppm)	24.43	Pb (ppb)	49.22	Sm (ppb)	69.41
V (ppb)	16.26	P (ppm)	27.23	Yb (ppb)	49.83	Er (ppb)	71.70
Cu (ppb)	17.39	Cs (ppb)	28.67	Br (ppb)	50.50	Tb (ppb)	72.21
Sb (ppb)	18.01	Co (ppb)	28.69	Ce (ppb)	56.60	Cl (ppm)	78.81
Ba (ppb)	19.95	Zn (ppb)	31.77	Hf (ppb)	59.23	Eu (ppb)	87.74
Ga (ppb)	20.45	Nb (ppb)	33.10	La (ppb)	61.24		
Fe (ppm)	21.27	Th (ppb)	34.83	Lu (ppb)	63.42		

Table 7. The average coefficient of variation, or CV_{AVG} (%) calculated from 4 field duplicate samples analysed by modified aqua-regia dissolution followed by inductively coupled plasma mass and emission spectroscopy. Green indicates good precision, blue indicates acceptable precision and red, marginal to poor precision. Boron, W and S values for the duplicate samples are at or below detection limit and have not been included in the analysis.

Element	CV_{avg} (%)						
U (ppm)	0.00	Cr (ppm)	8.58	Al (pct)	14.01	Ni (ppm)	19.14
Pb (ppm)	3.45	Ti (pct)	9.03	Na (pct)	14.82	Mn (ppm)	25.73
La (ppm)	5.86	Fe (pct)	9.33	Mg (ppm)	15.08	P (pct)	26.49
Sr (ppm)	6.21	Bi (ppm)	10.02	As (ppm)	15.61	Hg (ppb)	30.18
Th (ppm)	6.37	Te (ppm)	10.10	Ba (ppm)	15.61	Ag (ppb)	33.25
V (ppm)	7.29	Sc (ppm)	10.55	Co (ppm)	16.83	Se (ppm)	35.36
Ga (ppm)	7.87	Cd (ppm)	11.31	Cu (ppm)	17.20	Au (ppb)	72.25
Ca (pct)	8.04	K (pct)	11.52	Sb (ppm)	17.33		
Tl (ppm)	8.55	Zn (ppm)	13.56	Mo (ppm)	17.78		

6. Results

6.1 System functionality

The Leech River test provided an initial estimate of CO₂ and O₂ measurement reliability. At Leech River site 1, close to the projected trace of a thrust fault, CO₂ and O₂ concentrations, pressure, temperature and humidity were measured at 10-second intervals over 10 minutes. CO₂ was measured twice to confirm system functionality. The mean and RSD% values of CO₂ and O₂ at site 1 are listed in Table 8 and 9, respectively,

Table 8. Mean and percent relative standard deviation (RSD%) of CO₂, number of measurements (N), pressure, temperature and humidity measured at 10-second intervals in atmospheric air and soil gas at Leech River Site 1. Two CO₂ measurement sequences were collected at this calibration site to test measurement reliability. Atmospheric air measurements occur before and after each soil gas determination to establish a CO₂ background concentration.

Measurement	N	CO ₂ ppm	CO ₂ RSD%	Pressure mbar	Pressure RSD%	Temp. °C	Temp. RSD%	Humidity %	Humidity RSD%
Mean atmospheric air 1	10	416.4	7.1	941.7	0.4	22.3	1.5	41.5	2.5
Mean soil gas 1	13	9452.3	4.2	940.7	0.1	21.7	1.8	42.1	3.4
Mean atmospheric air 2	11	519.1	21.8	940.5	0.1	21.3	1.2	42.3	2.4
Mean soil gas 2	12	9487.7	16.4	939.6	0.1	20.8	2.4	42.9	4.6
Mean atmospheric air 3	14	569.2	7.4	939.5	0.1	20.8	2.1	44.9	1.5

Table 9. Mean and percent relative standard deviation (RSD%) of O₂, pressure, temperature and humidity measured at 10-second intervals in atmospheric air and soil gas at Leech River Site 1.

Measurement	N	O ₂ ppm	O ₂ RSD%	Pressure mbar	Pressure RSD%	Temp. °C	Temp RSD%	Humidity %	Humidity RSD%
Mean atmospheric air 1	17	206826	0.7	911.8	0.2	20.4	0.7	44.4	3.6
Mean soil gas 1	13	197410	0.5	907.2	0.2	20.7	0.3	46.8	3.6
Mean atmospheric air 2	14	204645	0.3	913.4	0.1	20.8	0.2	48.8	2.7

Tables 8 and 9 show that the RSD% values for most CO₂, O₂, pressure, temperature and humidity measurements are small and survey results are reliable. The exception is the RSD% of 22 for the second atmospheric air measurement and RSD% of 16 for the second soil gas measurement, affected by several increasing CO₂ measurements during a change from atmosphere to soil gas (16:20 hours; Figure 7). These values likely indicate the mixing of soil gas and atmosphere during the change. A spike in soil gas CO₂ concentration followed by a slower decline, then stabilization occurs at the beginning of some soil gas measurements (Figure 7). The CO₂ spike does not appear in every measurement and the reason for the initial anomalous reading is unknown. The spike concentration is not included in the mean and RSD% calculation.

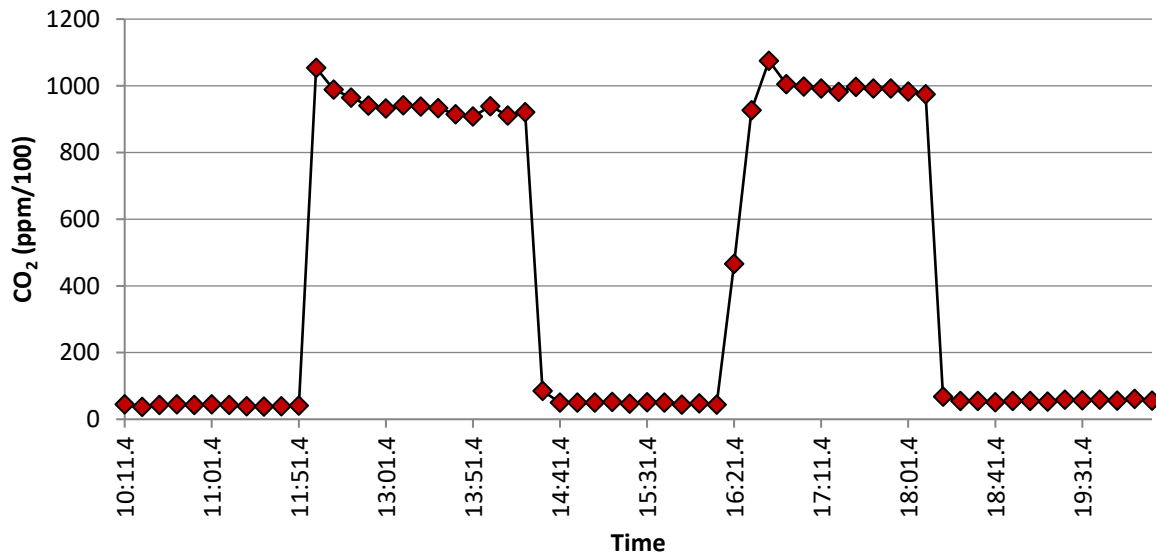


Figure 7. Soil gas and atmospheric air CO₂ concentrations at Leech River Site 1. Low zones are atmosphere measurements; high zones are soil gas measurements. Note the ‘spike’ anomaly that occurs at the beginning of each soil-gas measurement.

An examination of relationships between CO₂ and O₂ concentration, pressure, temperature and humidity measurements at the Leech River site revealed that there is no statistical correlation between soil gas CO₂ concentrations and other variables. There does, however, appear to be a correlation with low pressure and low soil gas O₂. In atmosphere, higher CO₂ is related to lower temperature and higher humidity. Since pressure, temperature and humidity seem only to affect atmospheric CO₂ concentrations, there appears to be no mixing of soil gas and the atmosphere during sampling. Figure 8 shows that the highest ΔCO₂&O₂ levels are detected in the soil gas measured closest to the Leech River thrust fault and values are generally lower to the south.

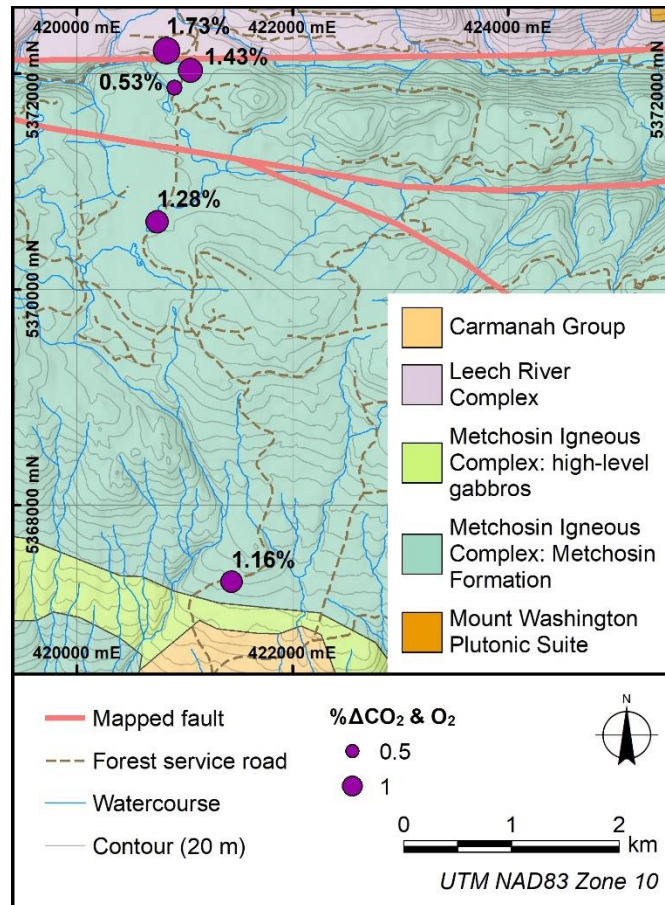


Figure 8. Percent ΔCO_2 & O_2 values measured at the Leech River sites.

6.2 Diurnal variation test

Atmospheric and soil gas CO_2 and O_2 concentrations measured every 2 to 3 hours between 9:00 and 22:00 hours show that both gas levels fall during the day and increase in the evening (Table 10; Figure 9). The RSD% value of the gas measurements is greatest for atmospheric CO_2 (29%), smaller for soil gas (18%) and smallest for the O_2 measurements (0.45%). An atmospheric CO_2 difference of 165 ppm is measured between 13:20 hrs and 20:32 hrs while the soil gas CO_2 changes by 889 ppm over the same time interval (Figure 9). The highest soil gas CO_2 concentration measured was at 20:32 hrs. Oxygen concentrations in soil gas over the same time interval increase by 519 ppm, but only 62 ppm in the atmosphere. The CO_2 concentration varies by an average of 200 ppm between 9:00 and 16:45 hrs, which is considered small. Therefore, it is interpreted that the effect of diurnal changes on survey results are minimal when soil gas measurements are made during the day, roughly between 9:00 hrs and 16:45 hrs.

Table 10. Mean and of relative standard deviation (RSD%) for CO₂ and O₂ measured at 10-second intervals in atmosphere and soil gas for an average 2 minutes at Victoria, BC on August 10, 2019.

Time (hours)	9:00	13:20	16:45	19:40	20:32	22:00
CO ₂ atmosphere (ppm)	409	254	255	344	419	401
RSD CO ₂ atmosphere (%)	14	29	24	20	8	21
CO ₂ soil gas (ppm)	1749	1424	1502	1744	2313	1914
RSD CO ₂ soil gas (%)	4	11	18	13	3	4
O ₂ atmosphere (ppm)	209753	209244	208561	209074	209182	208605
RSD O ₂ atmosphere (%)	0.12	.04	0.45	0.12	0.1	0.12
O ₂ soil gas (ppm)	201638	207439	206606	207608	207958	207272
RSD O ₂ soil gas (%)	0.22	0.44	0.34	0.25	0.33	0.26

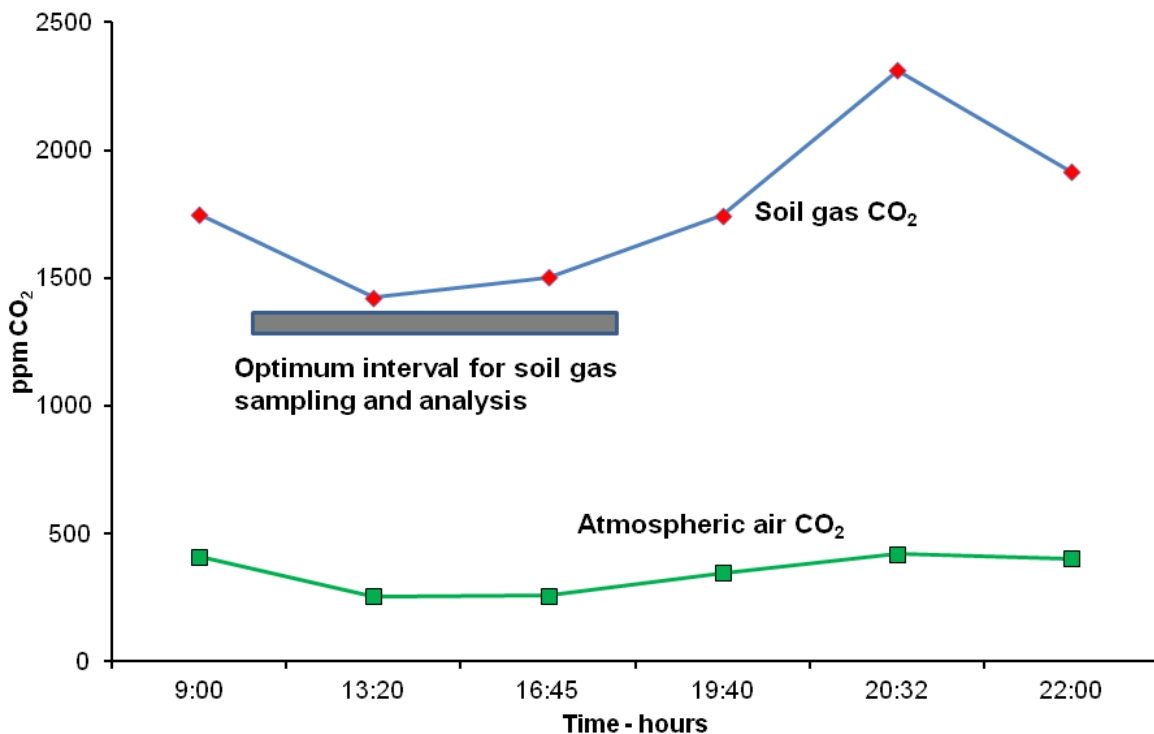


Figure 9. Measured soil gas and atmosphere CO₂ concentrations near Victoria, BC on August 10, 2019.

6.3 Field tests

6.3.1 Summary statistics for soil geochemistry

Summary statistics for IDH factors and element concentrations in the Mouse Mountain and Shiko Lake soils are presented in Tables 11 and 12. These tables also include the number of outlier samples (i.e., samples with values exceeding the 3rd quartile + 1.5 interquartile range), indicating that they are

considered anomalous. Several of the elements and IDH factors have more than one outlier, but only As and Cu have more than 5 by both WL-ICP-MS and AR-ICP-MS/ES.

Table 11. Summary statistics for elements determined in the Mouse Mountain and Shiko Lake soil samples by water leach followed by inductively coupled plasma mass spectroscopy (WL).

Element	Analysis	Minimum	Median	Mean	Maximum	1 st Q	3 rd Q	IQR	3Q+(1.5 IQR)	Outliers (n)
IDH	n/a	32	90	134	833	56	122	66	220	5
Ag (ppb)	WL	0.5	0.3	0.5	4.1	0.3	0.3	0	0.3	1
Al (ppm)	WL	9	18	19	39	14	22	8	34	1
As (ppb)	WL	5	19	22	95	13	24	12	42	5
Ba (ppb)	WL	97	281	346	1072	193	467	274	877	1
Ca (ppm)	WL	11	40	43	177	29	47	18	74	2
Co (ppb)	WL	3	8	10	28	6	12	6	21	5
Cu (ppb)	WL	20	51	90	871	34	78	44	144	6
Fe (ppm)	WL	6.1	13.2	14	24.1	10.8	17.2	6.4	26.8	1
Ga (ppb)	WL	1.3	3.2	3.9	9.8	2.4	4.9	2.5	8.5	0
K (ppm)	WL	10	31	33	99	24	37	13	56.5	3
Mg (ppm)	WL	3.4	8.1	8.7	22.3	5.9	9.9	4.1	16.1	4
Mn (ppb)	WL	157	544	897.3	4486	348	898.5	550.5	1724.3	5
Mo (ppb)	WL	0.5	5	5.7	33	4	6	2	9	2
Na (ppm)	WL	3	3	3	13	1	5	4	11	1
Ni (ppb)	WL	5	20	23	76	15	27	12	45	2
P (ppm)	WL	8.5	20.5	21.9	45.4	15.7	28.5	12.8	47.7	0
Pb (ppb)	WL	3	3	3	8	1	4	3	9	0
S (ppm)	WL	10	10	11	21	10	10	0	21	0
Sb (ppb)	WL	1	5	5	13	3	6	3	11	0
Sr (ppb)	WL	63	150	160	403	116	179	64	274	2
Ti (ppm)	WL	0.2	0.6	0.6	1.4	0.4	0.7	0.3	1.1	3
V (ppb)	WL	50	85	84	137	68	104	36	158	0
Zn (ppb)	WL	18	94	98	291	57	120	63	214	2

Table 12. Summary statistics for elements determined in the Mouse Mountain and Shiko Lake soil samples by a modified aqua-regia dissolution followed by inductively coupled plasma mass and emission spectroscopy (AR).

Element	Analysis	Minimum	Median	Mean	Maximum	1 st Q	3 rd Q	IQR	3Q+(1.5 IQR)	Outliers (n)
IDH	n/a	32	90	134	833	56	122	66	220	5
Ag (ppb)	AR	31	101	114	499	74	136	62	229	1
Al (pct)	AR	0.43	1	1.3	3.8	0.8	1.8	1.1	3.4	1
As (ppm)	AR	1.1	3.3	5.3	24.6	2.4	4.8	2.5	8.5	5
Ba (ppm)	AR	30	84.7	94.2	182.8	71.4	112.2	40.8	173.3	1
Ca (ppm)	AR	1200	2950	3653	17100	2675	3425	750	4550	5
Co (ppm)	AR	1.7	6.5	7.6	28.1	4	10.4	6.4	19.9	1
Cu (ppm)	AR	4.4	13.5	27.1	206.6	10.3	20.2	9.9	35.1	6
Fe (ppm)	AR	8600	20300	22400	69100	14800	29400	14600	51200	1
Ga (ppm)	AR	2.5	4.8	5.2	12.5	3.7	6.4	2.7	10.3	2
K (ppm)	AR	400	600	735	1400	500	1000	500	1750	0
Mg (ppm)	AR	900	2850	4370	18900	2150	6000	3850	11775	2
Mn (ppm)	AR	63	215	309	989	171	375	205	682	4
Mo (ppm)	AR	0.3	0.5	0.6	1.6	0.4	0.7	0.3	1.2	1
Na (ppm)	AR	60	80	81	100	78	90	13	109	0
Ni (ppm)	AR	3.7	13.3	20.4	74.2	9.3	25.8	16.5	50.7	3
P (ppm)	AR	170	610	698	2080	445	790	345	1308	3
Pb (ppm)	AR	3.9	4.8	5.9	17.8	4.3	6.1	1.8	8.8	5
S (pct)	AR	0.01	0.01	0.01	0.02	0.02		0	0.01	2
Sb (ppm)	AR	0.1	0.2	0.2	0.5	0.1	0.3	0.1	0.4	1
Sr (ppm)	AR	12.1	19.1	26.5	60.2	16.6	34.7	18.1	61.9	0
Ti (ppm)	AR	380	685	767	2850	640	803	163	1046	3
V (ppm)	AR	34	55	61	237	48	65	17	90	2
Zn (ppm)	AR	17.5	49.9	69.4	185.4	38.2	90.9	52.7	170	2

6.3.2 Mouse Mountain

The Pearson correlation coefficients for selected elements in the Mouse Mountain soil data are presented in Table 13. Soil gas, soil pH and soil IDH results from 30 soil samples from Mouse Mountain by a WL show a significant, positive correlation (> 0.7) between Sr (WL) and Ca (WL), and Zn (WL) and Mn (WL). There are weaker, positive correlations (> 0.5) between: S (WL) and $\Delta\text{CO}_2\text{-O}_2$; pH and Cu (AR); Mo (AR); Cu (AR) and Mo (AR); Cu (WL) and Mo (WL); Cu (WL) and Sr (WL); Mo (WL) and Sr (WL); and Mo (WL) and Ca (WL). Most correlations were found between the WL data with only Cu and Mo correlating in the AR data. There were no positive correlations between results from different analytical methods.

Table 13. Pearson correlation matrix for select element and soil-gas concentrations, pH and inverse difference hydrogen factors (IDH) of 30 soil samples from Mouse Mountain study area (blue text: elements analysed by water leach followed by inductively coupled plasma mass spectroscopy; black text: elements analyzed by modified aqua-regia dissolution followed by inductively coupled plasma mass and emission spectroscopy). Correlation coefficients > 0.7 are identified in red text) and > 0.5 in green.

	ΔCO_2 & O_2	pH	IDH	Ca	S	Sr	Mn	Cu	Cu	Mo	Mo	Zn	Ag
ΔCO_2 & ΔO_2	1.00	-0.06	0.07	-0.14	0.58	-0.12	-0.34	0.33	0.12	0.05	-0.06	-0.17	0.05
pH	-0.06	1.00	-0.02	0.50	-0.16	0.50	0.13	0.45	0.53	0.50	0.33	-0.01	0.21
IDH	0.07	-0.02	1.00	0.10	0.20	0.03	-0.15	0.06	-0.14	0.19	-0.23	-0.15	-0.03
Ca	-0.14	0.50	0.10	1.00	0.19	0.72	0.32	0.35	0.17	0.55	0.02	0.30	0.35
S	0.58	-0.16	0.20	0.19	1.00	0.21	-0.11	0.49	-0.08	0.21	-0.31	-0.01	0.06
Sr	-0.12	0.50	0.03	0.72	0.21	1.00	0.44	0.58	0.25	0.64	0.22	0.42	0.29
Mn	-0.34	0.13	-0.15	0.32	-0.11	0.44	1.00	0.09	0.13	0.15	0.19	0.80	0.07
Cu	0.33	0.45	0.06	0.35	0.49	0.58	0.09	1.00	0.64	0.55	0.23	0.09	0.25
Cu	0.12	0.53	-0.14	0.17	-0.08	0.25	0.13	0.64	1.00	0.29	0.67	-0.02	0.27
Mo	0.05	0.50	0.19	0.55	0.21	0.64	0.15	0.55	0.29	1.00	0.06	0.17	0.17
Mo	-0.06	0.33	-0.23	0.02	-0.31	0.22	0.19	0.23	0.67	0.06	1.00	0.07	0.07
Zn	-0.17	-0.01	-0.15	0.30	-0.01	0.42	0.80	0.09	-0.02	0.17	0.07	1.00	0.18
Ag	0.05	0.21	-0.03	0.35	0.06	0.29	0.07	0.25	0.27	0.17	0.07	0.18	1.00

At Mouse Mountain, the southernmost ΔCO_2 & O_2 soil-gas value (site 1101), measured over the previously mapped northeast-southwest fault, was less than 2% (Figure 10a), suggesting an absence of structural influence on the soil-gas concentrations. Sampling 50 m north of the mapped fault on the same transect, however, detected ΔCO_2 & O_2 values up to 5%. It is known that the location of the fault is poorly constrained, and the real-time measurements suggested the fault system is farther north, thus more closely spaced samples were taken in that area to ensure that the structure was not missed by the survey.

The highest ΔCO_2 & O_2 soil-gas values occur along the westernmost transect (Figures 10a). From these peaks, ΔCO_2 & O_2 values between 2 and 3% extend along northeast trends across the three transects (Figure 10a). These results suggest the occurrence of a concealed fault or fracture system north of the fault location mapped by Schimann (2014). Black dashed lines on Figures 10 and 11 estimate the location of structural features as indicated by the soil-gas measurements and are referred to as inferred faults. Elevated soil IDH factors are present (Figure 10b) at sites on the west and centre transects, and at some of the sites higher IDH corresponds to the high soil-gas ΔCO_2 & O_2 .

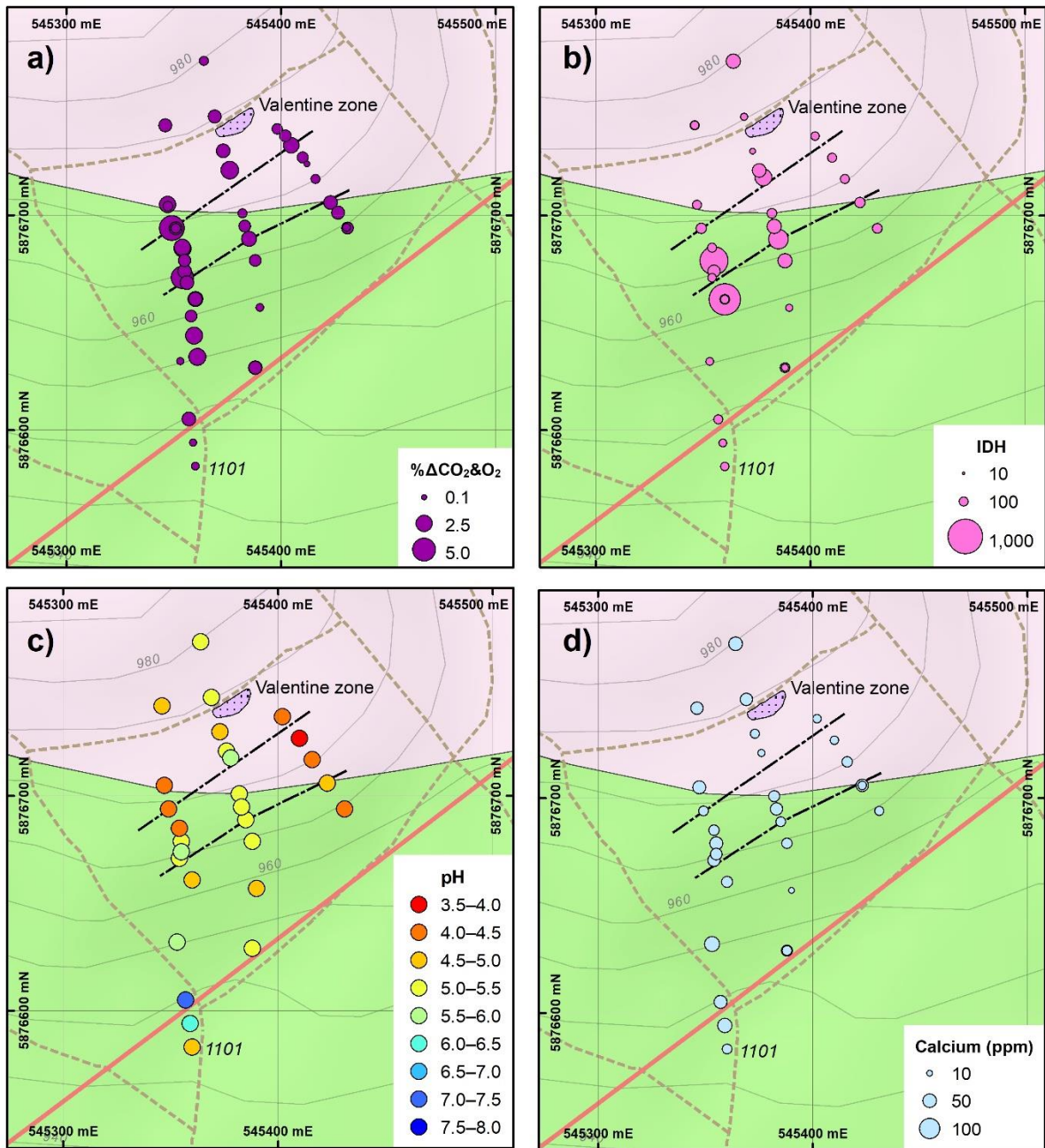


Figure 10. Mouse Mountain analytical results: a) soil gas $\Delta\text{CO}_2\&\text{O}_2$ in percent; b) inverse difference hydrogen ion factor (IDH); c) soil pH; and d) soil calcium (water leach extraction followed by inductively coupled plasma mass spectroscopy). Background: simplified bedrock geology from Schimann (2014). Symbol sizes for A, B and D are true proportional scales of the sample value.

The variation of soil pH shows no obvious relationship to the location of two fault structures inferred from the results of this study. There is, however, a stronger spatial association between higher IDH and structure, especially on the west and central transects. Higher soil Ca (AR) concentrations also correspond to one of the inferred structures, although there are scattered C anomalies on other transects. Anomalous water-soluble Cu (WL) concentrations (Figure 11b) cluster towards the south end of the west transect, corresponding to elevated IDH Ca (AR) concentrations. The highest water-soluble S concentrations up to 21 ppm are clustered on the west transect, close to the south inferred fault (Figure 11b).

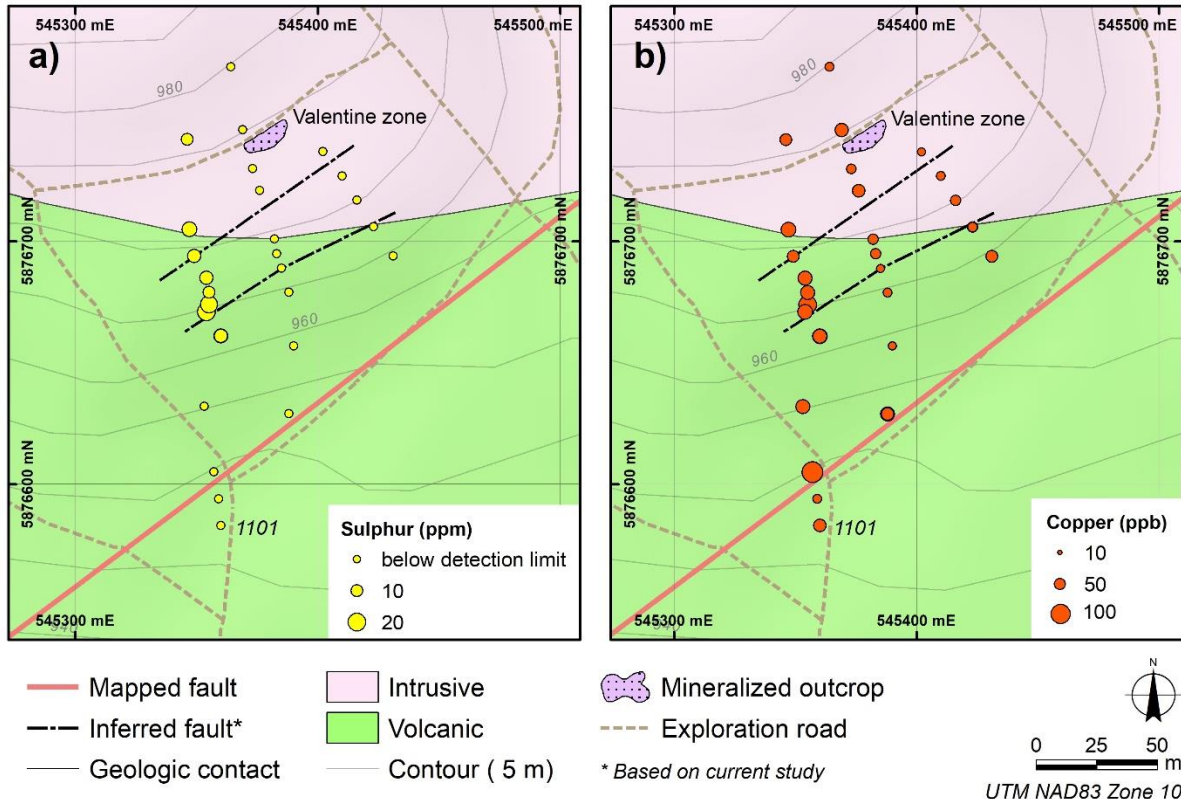


Figure 11. Mouse Mountain analytical results: a) soil sulphur; and b) soil copper by water leach extraction followed by inductively coupled plasma mass spectroscopy. Simplified bedrock geology from Schimann (2014). Symbol sizes are true proportional scales of the sample value.

On the Mouse Mountain centre transect (Figure 12), higher IDH factors correspond to the elevated $\Delta\text{CO}_2\&\text{O}_2$ peaks, whereas the $\Delta\text{CO}_2\&\text{O}_2$ peaks flank a single high IDH value on the west transect (Figure 13). There are lower water-soluble Ca concentrations associated with the $\Delta\text{CO}_2\&\text{O}_2$ peaks on both transects and the negative water-soluble Ca peak is most correlative on the centre transect (Figure 12). Anomalous S by WL values correspond to the $\Delta\text{CO}_2\&\text{O}_2$ peaks on the western transect (Figure 13), but there are no detectable S concentrations in the centre transect (Figure 12). Other trace elements (not shown in the figures) such as Sr (WL), display peaks with Ca (WL) and $\Delta\text{CO}_2\&\text{O}_2$ whereas Mn (WL), Fe (WL) typically show troughs where there are Ca (WL) and $\Delta\text{CO}_2\&\text{O}_2$ peaks.

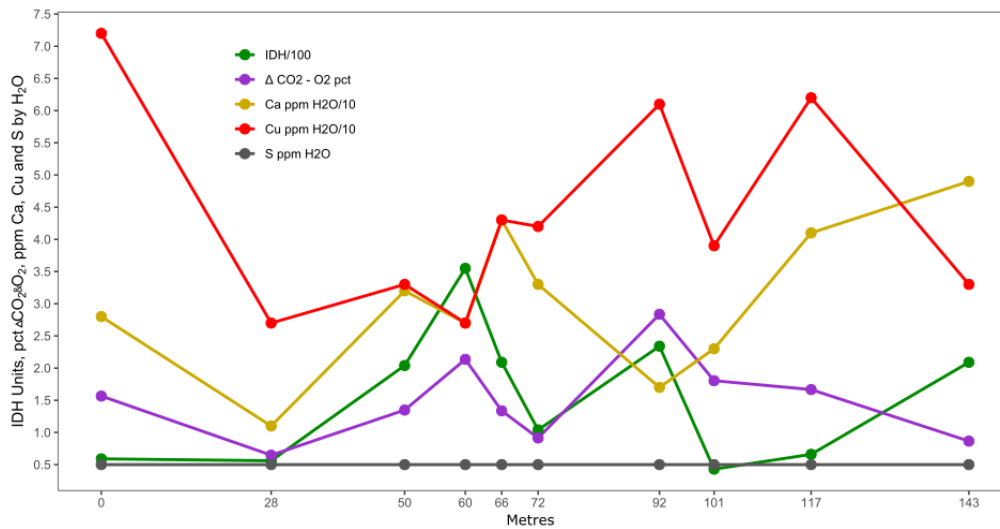


Figure 12. Soil-gas $\Delta\text{CO}_2\&\text{O}_2$ in percent, inverse difference hydrogen ion (IDH) factor with Ca, Cu and S concentrations (water leach extraction followed by inductively coupled plasma mass spectroscopy) in soil along the Mouse Mountain centre transect.

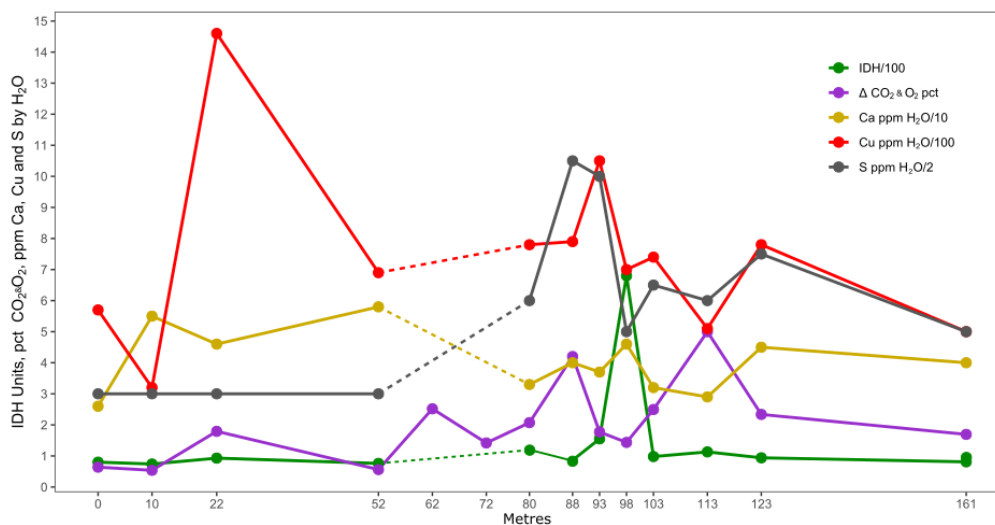


Figure 13. Soil gas $\Delta\text{CO}_2\&\text{O}_2$ in percent, inverse difference hydrogen ion (IDH) factor with Ca, Cu and S (water leach extraction followed by inductively coupled plasma mass spectroscopy) in soil along the Mouse Mountain west transect.

6.3.3 Shiko Lake

The Pearson correlation coefficient from selected elements in the Shiko Lake soil data are presented in Table 14. Although the number of analyses is small, soil gas, pH and IDH results from the 14 soil samples from Shiko Lake by WL and AR show multiple significant correlations (> 0.7) (Table 14; red entries). Strong correlations occur between IDH with Cu (WL) and Mo (WL); Ca (WL) with Sr (WL), Cu (WL), Cu (WL) with Mo (WL) and Ag (AR); Mo (WL) with Sr (WL) and Ag (AR); and Zn (WL) with Sr (WL) and Mn

(WL). Weaker correlations are identified by green entries in Table 14 but should be considered tentative due to the low number of samples. In general, there are stronger base metal associations in the Shiko Lake data than in the Mouse Mountain data.

Table 14. Pearson correlation matrix for select element and soil gas concentrations, pH and inverse difference hydrogen factors (IDH) of 14 soil samples from Shiko Lake study area (blue text: elements analysed by water leach followed by inductively coupled plasma mass spectroscopy; black text: elements analyzed by modified aqua-regia dissolution followed by inductively coupled plasma mass and emission spectroscopy). Correlation scores > 0.7 are identified in red text and > 0.5 in green.

	$\Delta\text{CO}_2\&\Delta\text{O}_2$	pH	IDH	Ca	S	Sr	Mn	Cu	Mo	Zn	Ag
$\Delta\text{CO}_2\&\Delta\text{O}_2$	1	0.13	0	0.02	0.02	-0.02	-0.2	0.06	0.08	0	0.07
pH	0.13	1	0.26	0.1	0.01	0.07	-0.09	0.28	0.18	0.16	0.31
IDH	0	0.26	1	0.65	0.31	0.47	0.21	0.72	0.72	0.31	0.62
Ca	0.02	0.1	0.65	1	0.69	0.92	0.21	0.84	0.93	0.53	0.88
S	0.02	0.01	0.31	0.69	1	0.64	0.04	0.52	0.62	0.36	0.66
Sr	-0.02	0.07	0.47	0.92	0.64	1	0.4	0.62	0.74	0.72	0.77
Mn	-0.2	-0.09	0.21	0.21	0.04	0.4	1	0.07	-0.02	0.79	0.054
Cu	0.06	0.28	0.72	0.84	0.52	0.62	0.07	1	0.93	0.32	0.87
Mo	0.08	0.18	0.72	0.93	0.62	0.74	-0.02	0.93	1	0.3	0.92
Zn	0	0.16	0.31	0.53	0.36	0.72	0.79	0.32	0.3	1	0.49
Ag	0.07	0.31	0.62	0.88	0.66	0.77	0.05	0.87	0.92	0.49	1

The $\Delta\text{CO}_2\&\Delta\text{O}_2$ soil-gas levels and IDH results increase to a peak over the siltstone at the Shiko Lake Quarry zone (Figure 14a,b). Coincidentally, pyrite-bearing siltstone float was observed here. The highest $\Delta\text{CO}_2\&\Delta\text{O}_2$ soil-gas value is toward the north end of the transect, whereas the highest IDH values occur at the south end of the transect (Figure 14a,b). With the IDH anomalies, there are corresponding increases in soil pH and concentrations of Ca, S, Mo and Cu by WL and Ag by AR- (Figures 14b,c and 15).

At the Shiko Lake East zone transect, the highest $\Delta\text{CO}_2\&\Delta\text{O}_2$ soil-gas value is directly south of the mapped fault and the highest IDH value is directly north of the mapped fault (Figure 16a,b). Soil pH increases slightly in the centre of the East zone transect (Figure 16c), but the more alkaline soils do not correspond to the elevated IDH or soil gas $\Delta\text{CO}_2\&\Delta\text{O}_2$. Conversely, high Ca concentrations do coincide with more alkaline soil, but not with the increased soil gas $\Delta\text{CO}_2\&\Delta\text{O}_2$ at the south end of the transect (Figure 16d). While the $\Delta\text{CO}_2\&\Delta\text{O}_2$ and IDH anomalies are proximal to the mapped fault, the trace metal soil anomalies are generally farther north suggesting that they reflect clastic transport of mineralized bedrock in till (Figure 17).

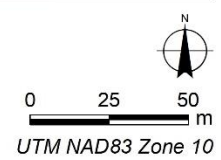
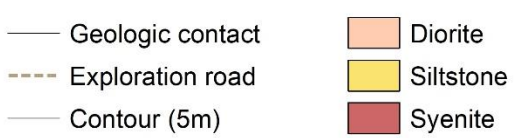
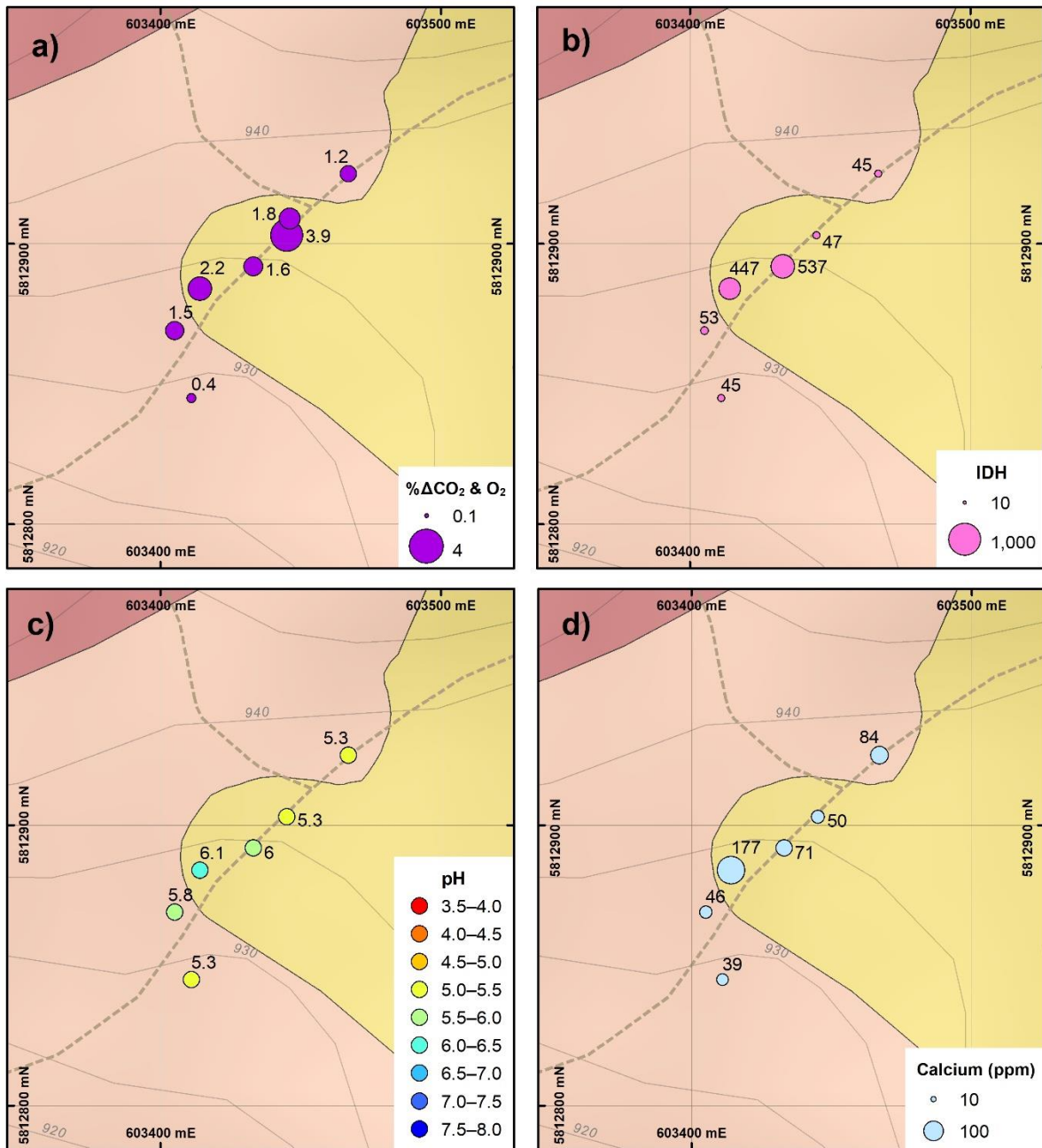


Figure 14. Shiko Lake Quarry zone analytical results: a) soil gas ΔCO_2 & O_2 in percent; b) inverse difference hydrogen ion factor (IDH); c) soil pH; and d) soil Ca determined by water leach followed by inductively coupled plasma mass spectroscopy.

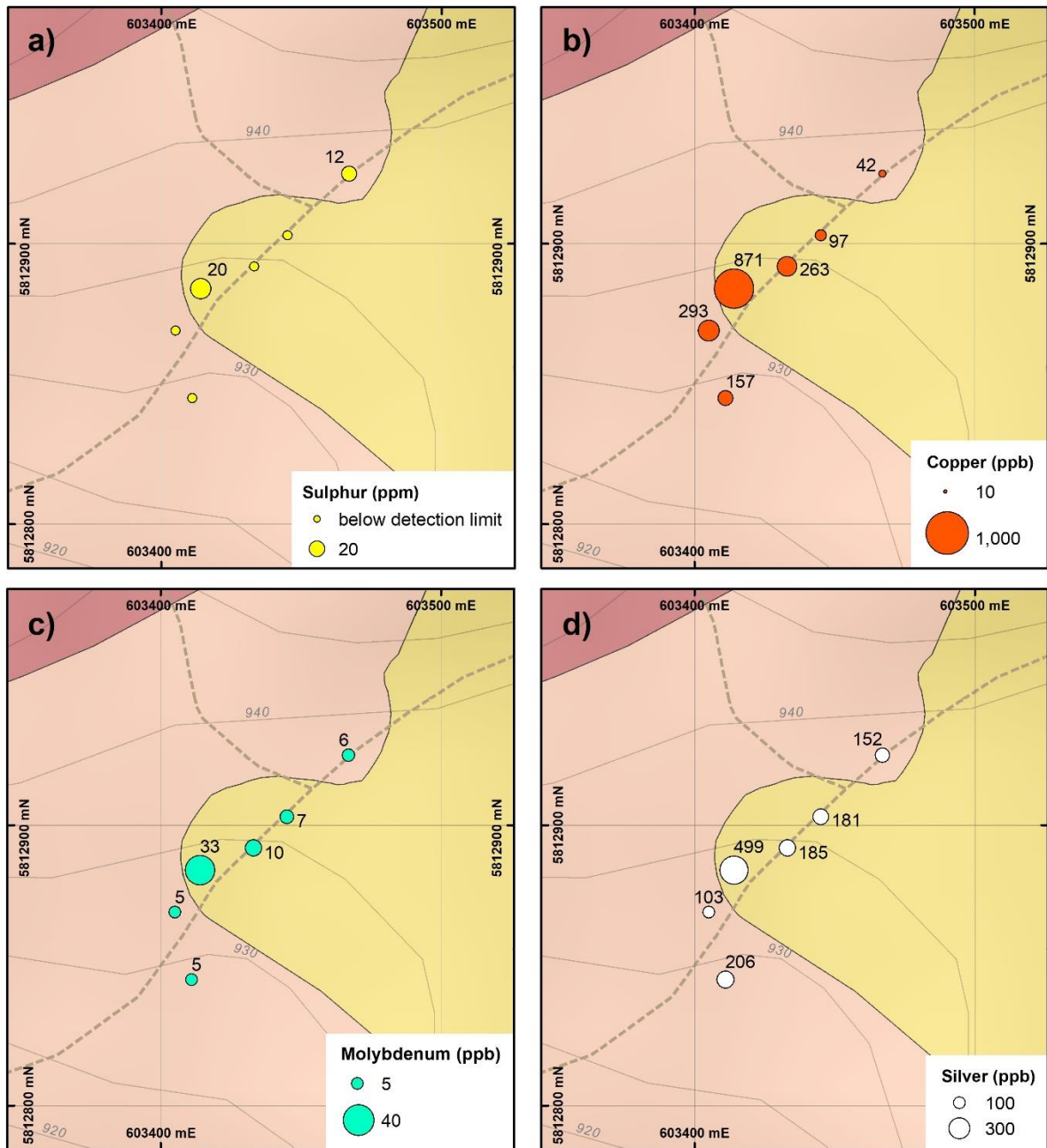


Figure 15. Shiko Lake Quarry zone analytical results: a) soil S; b) soil Cu; c) soil Mo; and d) soil Ag. S, Cu, Mo determined by water leach followed by inductively coupled plasma mass spectroscopy. Ag determined by modified aqua-regia dissolution followed by inductively coupled plasma mass or emission spectroscopy.

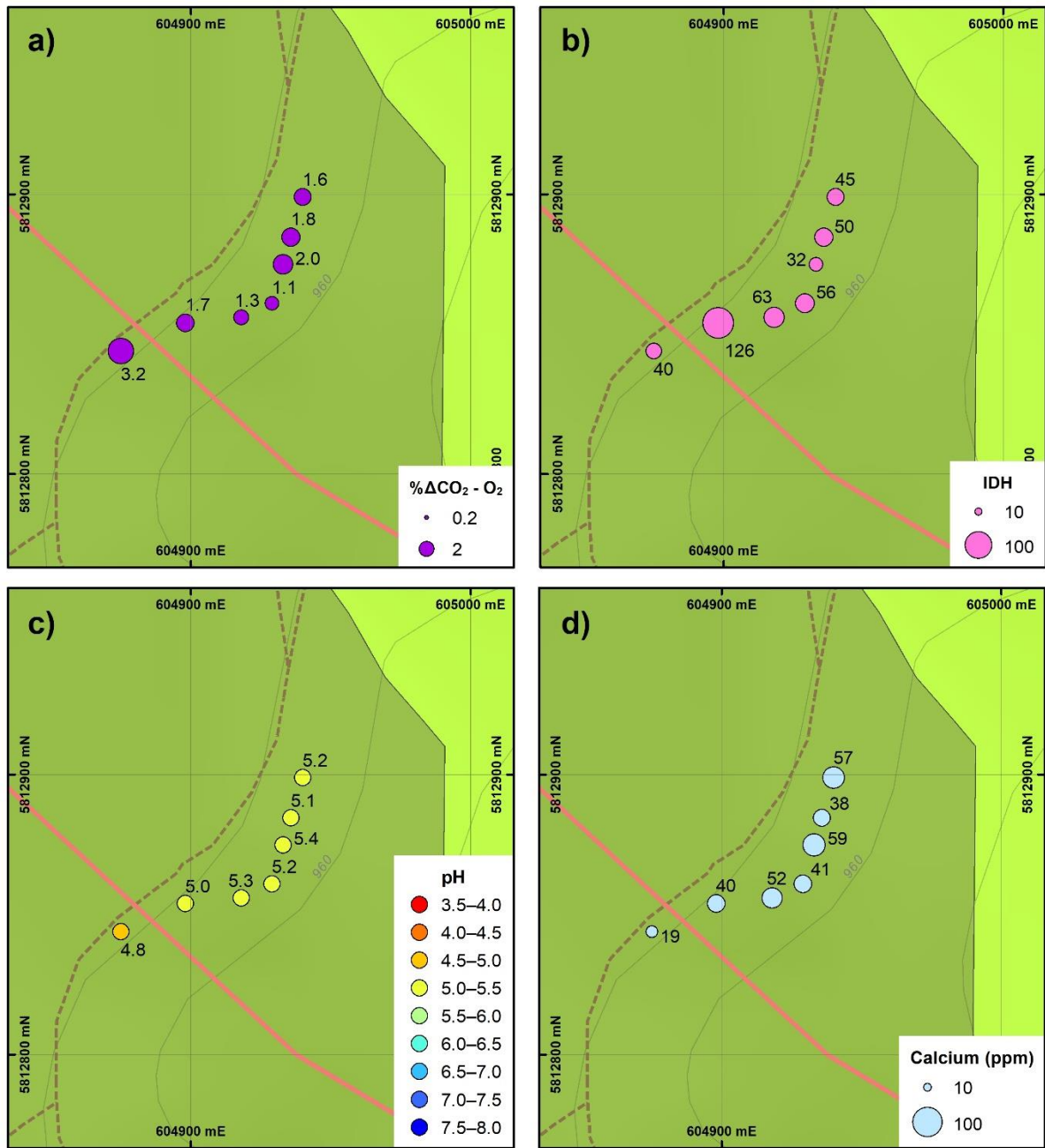


Figure 16. Shiko Lake East zone analytical results: a) soil gas ΔCO_2 & O_2 in percent; b) inverse difference hydrogen ion factor (IDH); c) soil pH; and d) soil Ca determined by water leach followed by inductively coupled plasma mass spectroscopy.

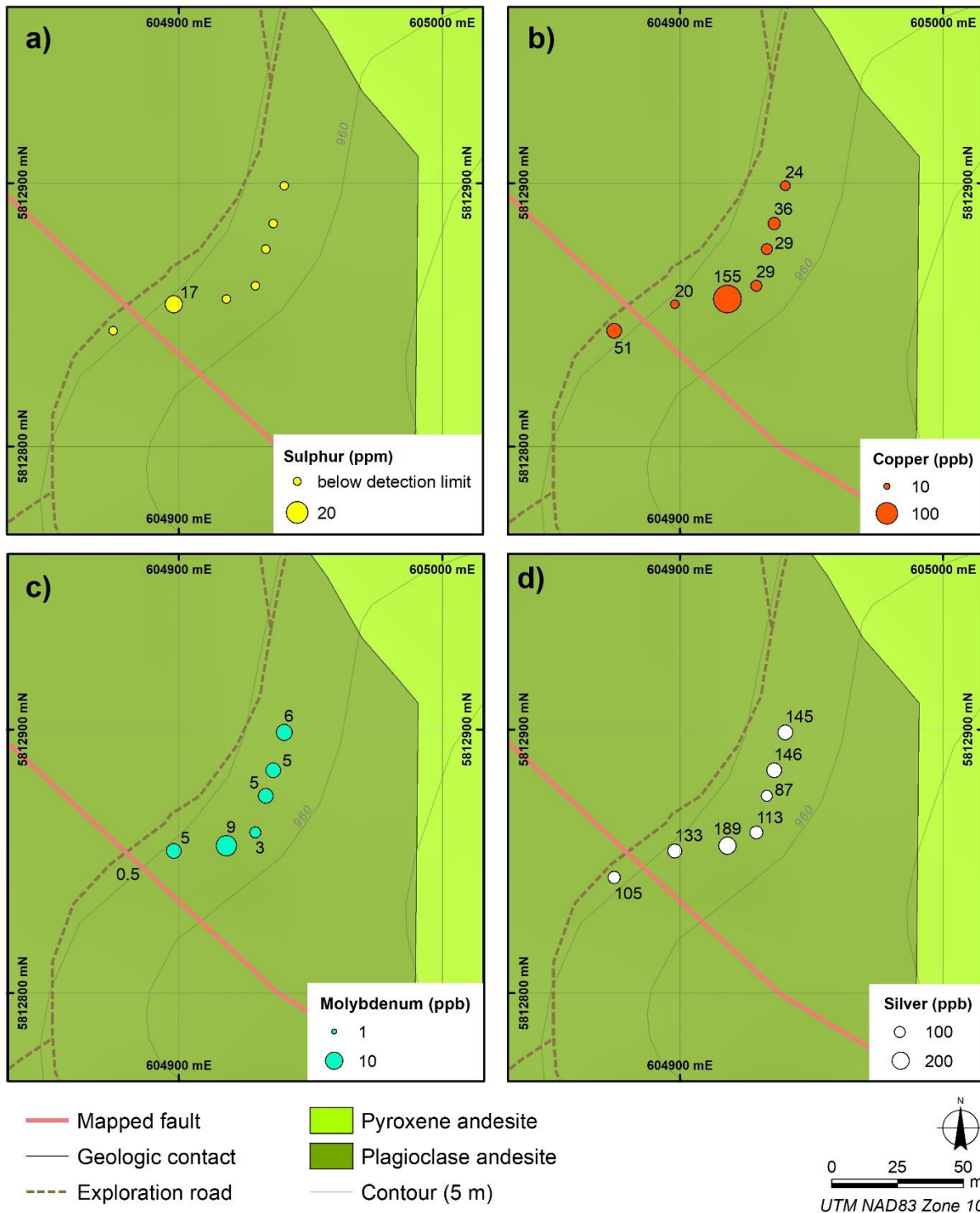
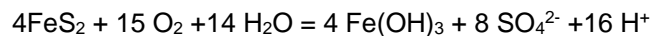


Figure 17. Shiko Lake East zone analytical results: a) soil S; b) soil Cu; c) soil Mo; and d) soil Ag. S, Cu, Mo determined by water leach followed by inductively coupled plasma mass spectroscopy. Ag determined by modified aqua-regia dissolution followed by inductively coupled plasma mass or emission spectroscopy.

7. Discussion

Field portable systems able to generate real time soil gas data have an advantage over passive gas collection units in that immediate results can inform sampling strategy modifications during a geochemical survey, thereby saving time and costs and improving results. Currently there are on-site analytical systems available for radon, methane, CO₂ and O₂. While these systems measure gas concentrations, they can be cumbersome, and for CO₂ and O₂, need separate units for measuring the individual gases. This project documents development and testing of a compact, field portable system for reliably measuring soil gas CO₂ and O₂ in one unit. The rationale for measuring these gases lies in the recognition that the variation of CO₂ and O₂ fluxes in soil can reflect the oxidization of sulphide minerals in bedrock and faults. This reaction will consume O₂ and decrease the gas flux through unconsolidated surficial sediment and soil with a concomitant increase in H⁺ ion concentration (pH decrease). Although the oxidation reaction is complex and mediated by bacteria it can be summarized overall by the following equation.



Calcite, if associated with a mineralized fault or hydrothermal alteration, will dissolve in the acid produced from the sulphide oxidation to generate CO₂. The reaction for this can be expressed as:



In addition to CaCO₃ dissolution in vadose and ground water there are other sources of fault transported CO₂. In a review of global ¹³C from the isotope analysis of CO₂-rich springs in seismically active regions, Irwin and Barns (1980) concluded that mantle sources for the CO₂ were channeled by faults; the metamorphism of sedimentary carbonate rocks; and by the degradation of soil organic matter. Studies by Cameron (2013) and Brown et al. (2019) have shown that soil geochemical anomalies can be attributed to the chemistry of ground water "pumped" from deep bedrock through faults by seismic activity. Much of the CO₂ in soil will be generated from macro- and micro-biota respiration during the decay of soil organic matter as part of chemical weathering and soil formation: In temperate global regions typical of the British Columbia interior, research has shown that soil gas CO₂ concentrations may reach 3200 ppm at 40 cm depth in soil compared to 400 ppm in the atmosphere (Chen, et al., 2005). In moist soil, CO₂ will combine with water to form bicarbonate (HCO₃⁻) and carbonate (CO₃²⁻) ions. Depending on the pH, soil structures, texture, the microbial communities and ground and vadose water chemistry, these ions can react with dissolved Ca in soil pore spaces to form CaCO₃ and other carbonate minerals such as SrCO₃ (Versteegen, 2010). Calcite solubility in water is controlled by CO₂ partial pressure and by pH. Increasing CO₂ partial pressure will increase CaCO₃ solubility, whereas increasing pH will cause CaCO₃ to precipitate (Misra, 2012).

At several sites along the Mouse Mountain west and central transect there is a spatial association between the ΔCO₂&O₂ peaks, higher soil pH, increased water leach Ca and an elevated IDH factor. A high IDH factor, representing the inverse of the difference between the acidified and non-acidified H⁺ concentrations, was proposed by Smee (2009) to indicate increased soil carbonate remobilization and precipitation. Hence, elevated soil gas ΔCO₂&O₂, soil IDH and water-soluble Ca at Mouse Mountain could reflect secondary carbonate precipitation over buried faults or fracture zones.

Migration of CO₂ from bedrock to the surface may not follow a direct path; consequently, ΔCO₂&O₂ soil gas anomaly contrast reflects both permeability of the surficial deposits and the size of the bedrock fractures able to release gases. Soil gas ΔCO₂&O₂ patterns at Mouse Mountain suggest that two fractures extend from the western and eastern transect over a distance of ~100 m. It is possible that the highest CO₂ flux at the west end suggests more intense fracturing or a difference in the permeability of the overlying glacial sediments. The presence of elevated S with the higher Δ CO₂-O₂ soil-gas values, with a statistically significant correlation between these variables, may also suggest the presence of oxidizing sulphides in fractures releasing S-rich gases such as carbonyl sulphide with the CO₂ (*cf.* Hale, 2016).

Other processes, such as glacial entrainment and dispersal of mineralized bedrock and subsequent chemical dispersion of elements from till into soil, may be responsible for Cu, Mo and Ag geochemical anomalies identified during this study in both Mouse Mountain and Shiko Lake areas. At Mouse Mountain, elevated Cu concentrations by WL with elevated Ca by WL and higher pH could reflect immobilization of Cu in the soil. The higher Cu concentration in the soil, close to the location of a mapped fault at the south end of the west transect, has no ΔCO₂&O₂ soil-gas anomaly. There is also no significant increase of Cu in soil sampled close to the Mouse Mountain Valentine Cu-Au mineralized zone. Soil geochemistry from British Columbia assessment reports compiled by Blain et al. (2016) revealed that soil in the area of the soil gas sampling contained less than 50 ppm Cu and only samples with more than 75 ppm Cu are east of the Valentine zone. At the Shiko Lake East zone, there are ΔCO₂&O₂ soil gas and IDH anomalies near the mapped fault, but elevated S (WL), Cu (WL), Mo (WL) and Ag (AR) in the soil occur farther north. These metals may have been mobilized from metal-enriched, transported till into the soil by the migration of more acid ground water, rather than directly from a buried fault or mineralization. This indicates that the soil gas anomalies provide a more direct indication of the potential fault or mineralization than the soil geochemistry as the metals in soil are also affected by glacial dispersion. In summary, at Mouse Mountain anomalous soil gas ΔCO₂&O₂ levels are clearly associated with elevated soil IDH values, but there is a weak relationship with anomalous soil Cu. At Shiko Lake, however, the association between anomalous soil gas ΔCO₂&O₂ and IDH values is weaker, but the relationship to Cu, Mo, Ag and S anomalies in the soil is stronger. This difference could be explained by more structural control of the soil gas and trace metal geochemistry at Mouse Mountain and the Shiko Lake East zone, but a stronger expression of bedrock sulphides in the soil geochemistry at the Shiko Lake Quarry zone.

This discussion of the soil gas and soil trace element geochemistry has focused on trace element patterns that might be expected to reflect increased CO₂ flux from concealed faults. Other elements among those analysed by a water leach and a modified aqua regia may also show variations induced by the soil gas anomalies. For example, lower O₂ levels in the soil gas associated with increased CO₂ caused by the presence of oxidizing sulphides could result in lower redox and higher mobility of Fe and Mn. Whereas water extract analyses reveal that these elements vary from site to site, the patterns are not consistently related to ΔCO₂&O₂ soil-gas anomalies and are likely due to other soil chemistry changes such as the presence of decaying organic matter or transport of metal enriched sediment.

8. Conclusions

A project to detect bedrock mineralization and geological faults beneath glacial deposits in Central British Columbia by the on-site, real time soil gas analysis of CO₂ and O₂ demonstrates that:

- An economical, field portable compact system can be built for measuring and recording real-time atmospheric air and soil-gas CO₂ and O₂ concentrations using commercial electronic gas sensors. The estimated cost for the system - comprising two sensors installed in a waterproof case, a battery powered pump and a hollow, steel probe to sample gas from a 0.5 m depth in soil and sediments - is approximately CAN \$1,100.
- Carbon dioxide and O₂ concentrations in atmosphere and soil gas can be detected by the sensors and recorded by a connected laptop computer equipped with custom software. In addition to measuring CO₂ and O₂ concentrations the software also records barometric pressure, temperature and relative humidity. These variables are displayed graphically and recorded for further data analysis. System set-up, sampling of atmospheric air for calibration, sampling soil gas and data recording can generally be completed in 15 to 20 minutes at each sample location.
- Preliminary testing of the system revealed that, after calibration to atmospheric levels, the system reliably measured elevated CO₂ and lower O₂ concentration, expressed as percent ΔCO₂&O₂ in soil-gas sampled at sites across the Leech River fault near Jordan River, BC.
- Atmosphere and soil gas CO₂ and O₂ concentrations measured at intervals over a 12-hour period revealed that a diurnal variation in gas concentration would not compromise survey results provided that the sampling was carried out between 9.00 and 17.00 hours. However, diurnal variations throughout the year and short-term changes in barometric pressure should be considered.
- Sampling soil-gas over drift-covered sulphide-mineralized rock at the Mouse Mountain and Shiko Lake Cu-Au porphyry occurrences demonstrated that the variation in CO₂ and O₂ concentrations was spatially coincident with inferred structures or mineralization beneath glacial deposits. Increased levels of S by WL from soil samples are associated with ΔCO₂&O₂ anomalies that may reflect sulphur gases such as carbonyl sulphide produced from oxidizing sulphides in structures. Sulphide oxidation could also explain the decreased O₂ concentration in the soil gas over the inferred structures at Mouse Mountain.
- The inverse difference hydrogen (IDH) factor, at Mouse Mountain is spatially related to soil gas ΔCO₂&O₂ peaks. The relationship suggests that the increased CO₂ flow from bedrock, through the glacial deposits to the surface influences soil pH and the mobility of Ca in the soil. Lower water-soluble Ca over ΔCO₂&O₂ peaks may reflect precipitation of secondary carbonate minerals in the soil.
- Copper, Mo and Ag anomalies identified in the soil at Mouse Mountain and Shiko Lake are transposed from the soil gas and IDH anomalies. It is likely that the soil anomalies are sourced from glacially transported material, and therefore the soil gases provide a more direct indication of mineralization than the soil geochemistry.

9. Recommendations

- Other gases (e.g. mercury, radon, methane, carbonyl sulphide) have been detected in soil gas above sulphide mineralization and faults. Incorporation of additional available sensors for these gases would improve the ability of the present system to discriminate between different targets. The key to using sensors for other gases will be the availability of the custom software to convert gas measurements into standard units of concentration.
- Calibrate the system and interpretations by collecting soil gas measurements where the geological structure, style of mineralization and the surficial cover are better defined.
- Combine the sensors and pump into a single unit with Swagelok® type connectors to improve the link to the soil-gas sampler.
- Determine the cause of short-term fluctuations and spikes in soil gas measurements by comparing the soil moisture content with CO₂ and O₂ concentrations
- Assessment of the effects of soil moisture on soil gas measurements.
- Evaluate utility of real time soil gas CO₂ and O₂ measurements to geothermal exploration, earthquake prediction and in agriculture research.
- Analyse soil samples for Ca and other trace elements by a 1M ammonium acetate leach to determine if there are secondary carbonates associated with the increased flow of soil gas CO₂.

10. Acknowledgments

Funding for this project was provided by Geoscience BC. Permission from K. Schimann, CanAlaska Uranium, to access the Mouse Mountain property is appreciated. R. Durfeld, Durfeld Geological Management Ltd. very kindly provided transportation from Williams Lake to the Shiko Lake property; advised on sample transect sites; and helped with the soil and soil gas sampling. His assistance and hospitality during the fieldwork was very much appreciated by the authors. J. Houck, CO2Meter Inc., is thanked for patiently and promptly answering many questions about the CO₂ and O₂ sensors. Altech machining and repairs Ltd, Victoria, BC, kindly assisted with machining parts for the soil gas sampling probe. S. Cook is especially thanked for a very careful and constructive review of a preliminary draft of the report and comments from two anonymous reviewers improved the quality of the report.

11. References

- Abzalov, M.Z. (2008): Quality control of assay data: A review of procedures for measuring and monitoring precision and accuracy; *Exploration and Mining Geology*, v. 17, p. 1–14.
- Blaine, F.A., Hart, C.J.R. and Jenkins, S. (2016): Surficial geochemical exploration data for British Columbia Porphyry Copper Deposits; Geoscience BC, Report 2016-15.
- Brown, A.E., Winterburn P.A and Bissig, T. (2019): Identification of the expression of earthquake-induced surface flooding by groundwater using detailed regolith mapping at the buried Atlántida Deposit, northern Chile; *Geochemistry: Exploration, Environment, Analysis*, 19, p.474-486.
- BC Geological Survey (2019): MINFILE BC mineral deposits database; BC Ministry of Energy, Mines and Petroleum Resources, URL <<https://minfile.ca>> [November 2019].
- Cameron, I.M. (2013): From Chile to Nevada to the Athabasca basin: earthquake-induced geochemical anomalies from near-field to far-field; *Geochemistry: Exploration, Environment, Analysis*, 13, p. 41–51.
- CO2Meter Inc. (2015): GSS sensor user manual; CO2Meter Inc., 51 p URL <<http://www.co2meters.com/Documentation/Manuals/Manual-GSS-Sensors.pdf>> [November 2019].
- Chen, Molina, D.J. A. E., Clapp, C.E., Venterea, R.T. and Palazzo, A.J. (2005): Corn root influence on automated measurements of soil carbon dioxide concentrations, *Soil Science*, 170, p 779 - 787.
- Cui, Y., Miller, D., Schiarizza, P., and Diakow, L.J., 2017. British Columbia digital geology. British Columbia Ministry of Energy, Mines and Petroleum Resources, British Columbia Geological Survey Open File 2017-8, 9p. Data version 2018-04-05.
- Duddridge, G.A., Grainger, P. and Durrance, E.M. (1991): Fault detection using soil gas geochemistry; *Quarterly Journal of Engineering Geology*, v. 24, p. 427–435.
- Fletcher, W.K. (1981): Analytical methods in geochemical prospecting, *Handbook of Exploration geochemistry Volume 1*, Editor G.J.S Govett, 254 pp.
- Gingrich, J. E. (1984): Radon as a Geochemical Exploration Tool. *Journal of Geochemical Exploration*. Vol. 21, p. 19-39.
- Hale, M. (2010): Gas geochemistry and deeply buried mineral deposits: the contribution of the Applied Geochemistry Research Group, Imperial College of Science and Technology, London; *Geochemistry: Exploration, Environment, Analysis*, v. 10, no. 3, p. 261–267.
- Hall, G.E.M (1998): Analytical perspective on trace element species of interest in exploration, *Journal of Geochemical Exploration* 91, p 1-9.

- Hamilton, S.M., Cameron, E.M., McClenaghan, M.B. & Hall, G.E.M. 2004. Redox, pH and SP variation over mineralization in thick glacial overburden. Part I: methodologies and field investigation at Marsh Zone gold property. *Geochemistry Exploration, Environment, Analysis*, 4, 33–44.
- Highsmith, P. (2004): Overview of soil gas theory; *Explore*, no. 122, p. 1–15.
- Imasu, R and Tanabe, Y. (2018): Diurnal and Seasonal Variations of Carbon Dioxide (CO₂) Concentration in Urban, Suburban, and Rural Areas around Tokyo, *Atmosphere* 2018, 9, p.367-377.
- Irwin, W.P., and Barnes, I. (1980): Tectonic relations of carbon dioxide discharges and earthquakes, *Journal of geophysical research*, 85, p 3105–3121
- Jonnes, S. and Logan, J.M. (2007): Bedrock geology and mineral potential of Mouse Mountain, central British Columbia; in *Geological Fieldwork 2006*, BC Ministry of Energy, Mines and Petroleum Resources, BC Geological Survey, Paper 2007-1, p. 55–66, URL <http://cmscontent.nrs.gov.bc.ca/geoscience/PublicationCatalogue/Paper/BCGS_P2007-01-06_Jonnes.pdf> [November 2019].
- Klusman, R.W. (2009) Transport of ultra trace reduced gases and particulate, near surface oxidation, metal deposition and adsorption; *Geochemistry Exploration, Environment, Analysis*, 9, 203-213.
- Lesage, G. (2011): Assessment report on the Red gold property, Cariboo Mining Division, BC, NTS: 093A06W; BC Ministry of Energy, Mines and Petroleum Resources, Assessment Report Indexing System (ARIS), ARIS Report 32975, 755 p., URL <<https://aris.empr.gov.bc.ca/ArisReports/32975.PDF>> [November 2019].
- Lovell, J.S., Hale, M, and Webb, J.S. (1993). Soil air carbon dioxide and oxygen measurements as a guide to concealed mineralization in semi-arid and arid regions. *Journal of geochemical exploration*, 19, pp 305-317.
- Lovell, J.S., Hale, M. and Webb, J.S. (1979): Soil air disequilibrium as a guide to concealed mineralization at Keel, Eire; in *Prospecting in Areas of Glaciated Terrain, 1979: papers presented at a symposium organized by the Irish Association for Economic Geology and held in Dublin, Ireland, 26–29 August, 1979*, The Institute of Mining and Metallurgy, London, p. 45–50.
- Lovell, J.S., Hale, M. and Webb, J.S. (1980): Vapour geochemistry in mineral exploration; *Mining Journal*, 1990, p. 229–239.
- McCarthy, J.H., Lambe, R.N. and Dietrich, J.A. (1986): A case study of soil gases as an exploration guide in glaciated terrain: Crandon massive sulfide deposit, Wisconsin; *Economic Geology*, v. 81, p. 408–420.
- Misra, K.C. (2012): *Introduction to geochemistry*, Wiley-Blackwell, 438 pp.
- Morton, J.W. (2003): *Prospecting and a geological reconnaissance on the Red gold property*, Cariboo Mining Division, BC; BC Ministry of Energy, Mines and Petroleum Resources, Assessment

Report Indexing System (ARIS), ARIS Report 27046, URL <<https://aris.empr.gov.bc.ca/ArisReports/27046.PDF>> [November 2019].

Ovchinnikov, L.N., Sokolov, V.A., Fridman, A.I. and Yanitskii, I.N. (1972): Gaseous geochemical methods in structural mapping and prospecting for ore deposits. In *Geochemical Exploration, 1972, Proceedings of the fourth international geochemical exploration symposium, 1972*, editor, M.J. Jones, pp 177-182.

Schimann, K. (2014): Geology and geochemistry at the QM property, NTS: 93G 01, BC; BC Ministry of Energy, Mines and Petroleum Resources, Assessment Report Indexing System (ARIS), ARIS Report 35262, 28 pp.

Smee, B.W. (1998): A new theory to explain the formation of soil geochemical response over deeply covered gold mineralization in arid environments; *Journal of Geochemical Exploration*, v. 61, p. 149–172.

Smee, B.W. (2003): Theory behind the use of soil pH measurements as an inexpensive guide to buried mineralization, with examples; *Explore*, no. 118, p. 1–18.

Smee, B.W. (2009): Soil micro-layer, airborne particles, and pH: the Govett connection; in *Proceedings of the 24th International Applied Geochemistry Symposium, June 1–4, 2009, Fredericton, New Brunswick*, Eds. D.R. Lentz, K.G. Thorne and K.-L. Beal, v. 1, p. 91–95.

Versteegen, A. (2010): Biotic and abiotic controls on calcium carbonate formation in soils, Unpublished Ph. D Thesis, Cranfield University (UK), School of Applied Sciences, Department of Natural Resources, 230 pp.

Appendix A

Raw CO₂ and O₂ atmosphere and soil gas measurements

- A1. GBC_Report2020-07_Appendix A1 - Leech River Soil Gas Data.xlsx
- A2. GBC_Report2020-07_Appendix A2 - Mouse Mountain Soil Gas Data - Sites MM 1001 to 1117.xlsx
- A3. GBC_Report2020-07_Appendix A3 - Mouse Mountain Soil Gas Data - Sites MM 1201 to 1310.xlsx
- A4. GBC_Report2020-07_Appendix A4 - Shiko Lake Soil Gas Data - Sites SL 2101 to 2207.xlsx
- A5. GBC_Report2020-07_Appendix A5 - Diurnal Soil Gas Test Victoria.xlsx

Appendix B

Processed soil gas data

B1. GBC_Report2020-07_Appendix B - Soil Gas Measurement Summary.xlsx

Appendix C

Mouse Mountain and Shiko Lake soil sample descriptions

C1. GBC_Report2020-07_Appendix C - Soil sample descriptions and soil pH measurements.xlsx

Appendix D

Mouse Mountain and Shiko Lake soil geochemistry

D1. GBC_Report2020-07_Appendix D - Soil
Geochemical Data.xlsx